NASA Technical Memorandum 85940

Nonlinear Problems in Flight Dynamics

Gary T. Chapman and Murray Tobak

May 1984

National Aeronautics and
Space Administration

NASA Technical Memorandum 85940

Nonlinear Problems in Flight Dynamics

Gary T. Chapman
Murray Tobak, Ames Research Center, Moffett Field, California

National Aeronautics and
Space Administration

Ames Research Center
Moffett Field, California 94035

NONLINEAR PROBLEMS IN FLIGHT DYNAMICS

Gary T. Chapman and Murray Tobak

NASA Ames Research Center, Moffett Field, CA 94035

1. INTRODUCTION. One might ask, Why a paper on nonlinear flight dynamics at this conference? There are at least two ways that this conference, with its focus on nonlinear problems in control and fluid dynamics, can be viewed. The first involves the basic commonality of nonlinear problems in control and fluid dynamics, particularly in their underlying mathematical structure. The second concerns itself with potential sources of nonlinear problems arising in controlling a flight system dominated by nonlinear fluid-dynamic forces and moments. It is with the latter question, and its description in both physical and mathematical terms, that this paper deals. It should be noted that the mathematical approach taken, which emphasizes the qualitative features of the problem, is not the traditional one of the aerodynamics community. Finally, the mathematical exposition is not intended to be fully rigorous but rather, to be descriptive, indicating possibilities and directions for future research.

The paper is divided into three parts: (1) a brief formulation of flight dynamics is presented in Sec. 2 to provide a framework for the aerodynamic system to be controlled; (2) a broad description of the source and nature of aerodynamic phenomena that give rise to the nonlinear forces and moments acting on a flight vehicle, and a discussion of the underlying mathematical structure are presented in Sec. 3; and (3) illustrations of how these nonlinear forces and moments manifest themselves

in the flight-dynamic behavior are presented in Sec. 4. This work utilizes the concepts of mathematical modeling of nonlinear aerodynamics summarized in the paper by Tobak et al. [1] in this conference proceedings.

2. FORMULATION OF FLIGHT DYNAMICS. Flight dynamics is the field of research concerned with the dynamical behavior of vehicles in flight. It is the resultant of the interaction of four systems. The two most basic are the inertial system of the vehicle and the aerodynamic system acting on the vehicle. Two additional systems are the deformational characteristics of the vehicle and a control system. The various levels at which the systems may interact are shown in Fig. 1. At the simplest level we have the free flight of a rigid body in which the interaction is between the inertial and aerodynamic systems. The control system intervenes to modulate the interaction between the inertial and aerodynamic system so as to bring about a desired flight behavior. For vehicles that are undergoing deformation resulting from, say, some elastic or nonelastic response to the varying inertial and aerodynamic loads, or that are undergoing a shape change because of ablation, the additional system to account for this must be considered, as shown in the lower portion of Fig. 1. This new system requires a more sophisticated control system to arrive at a desired flight behavior. An example problem is the alleviation of loads caused by gusts which involves an overall aero-servo-elastic system. For the sake of simplicity, we will confine our discussion to the inertial and aerodynamic systems.

From a system standpoint, the close coupling between the inertial system and the aerodynamic system is shown in the block diagram of Fig. 2.

The inertial system provides the body orientation, that is, boundary conditions, to the aerodynamic system. The aerodynamic system, in turn, provides the forces and moments to the inertial system. The output of this interaction is both the aerodynamic response (forces, moments, and flow field) and the vehicle motion history. The inertial system for a rigid body has six degrees of freedom: three of rotation and three of translation. The equations of motion (in general six functional-differential equations) in a body-fixed coordinate system are

$$(m\vec{v})_t = f_{a_1}\left[\vec{v}_o^{\,t}(\xi), \vec{\Omega}_o^{\,t}(\xi)\right] + f_g + f_{T_1} \tag{2.1}$$

and

$$(I\vec{\Omega})_t + \vec{\Omega} \times I\vec{\Omega} = f_{a_2}\left[\vec{v}_o^{\,t}(\xi), \vec{\Omega}_o^{\,t}(\xi)\right] + f_{T_2} , \tag{2.2}$$

where m is the vehicle mass, $\vec{v}$ is the velocity vector, $\vec{\Omega}$ is the angular velocity vector, and I is the moment of inertia tensor. In these equations $(\ )_t$ implies differentiation with respect to time (t), and ξ is a dummy time variable. There are normally three sets of applied generalized forces and moments: those due to aerodynamics, f_{a_1} and f_{a_2}, thrust, f_{T_1} and f_{T_2}, and gravity, f_g. The thrust and gravitational forces are normally simple functions. However, the aerodynamic forces and moments (f_{a_1} and f_{a_2}) are functionals rather than functions; their instantaneous values depend on the history of the vehicle's motion. This functional dependence is indicated in (2.1) and (2.2) by the square bracket notation.

The aerodynamic force and moment system, which constitutes the major source of nonlinearity, is now considered in more detail. The

equations governing the motion of a compressible viscous fluid are a set of nonlinear partial differential equations. In vector form they can be expressed as

$$\frac{\partial E}{\partial t} + \frac{\partial F}{\partial x} + \frac{\partial G}{\partial y} + \frac{\partial H}{\partial z} = 0 \ , \tag{2.3}$$

where

$$E^T = [\rho, \rho u, \rho v, \rho w, \rho e] \ ,$$

$$F^T = [\rho u, \rho uu - \sigma_{xx}, \rho uv - \tau_{xy}, \rho uw - \tau_{xz}, \rho ue - \dot{q}_x - \sigma_{xx}u - \tau_{xy}v - \tau_{xz}w] \ ,$$

$$G^T = [\rho v, \rho uv - \tau_{xy}, \rho vv - \sigma_{yy}, \rho vw - \tau_{yz}, \rho ve - \dot{q}_y - \tau_{xy}u - \sigma_{yy}v - \tau_{yz}w] \ ,$$

$$H^T = [\rho w, \rho uw - \tau_{xz}, \rho uw - \tau_{yz}, \rho ww - \sigma_{zz}, \rho we - \dot{q}_z - \tau_{xz}u - \tau_{yz}v - \sigma_{zz}w] \ ,$$

and where ρ is the fluid density, u, v, and w are velocity components, and e is the internal energy. The stress tensor (σ's and τ's) has been left unspecified. In their most general form the stress tensor components would involve the pressure and the molecular viscosity of the fluid. When the stress tensor is written in this form, the equations are the full Navier-Stokes equations which are said to govern the flow field surrounding the vehicle and give rise to the nonlinear aerodynamic behavior that we will describe in the next section. At the present time, the full equations cannot be solved, even with the largest available computers, for practical aerodynamic problems involving even simple geometries. Hence, various approximations are normally employed. For inviscid problems, dropping the stress tensor yields the nonlinear Euler equations, for which a wide range of solutions have been obtained. On the other hand, for viscous problems, performing some form of averaging on the full equations removes the complexities that occur at high Reynolds numbers. These different approximations have various domains

of validity; however, it is not our purpose here to consider the governing equations themselves but to discuss the nonlinear aerodynamic flows that are their result. Before leaving the fluid-dynamic system, we should note that the boundary conditions needed for this system are those of no flow through the vehicle surface and (for the full equations) no slip at the surface, and that all disturbances produced at the surface decay at large distances from the vehicle. The boundary conditions couple the aerodynamic system to the inertial system.

To conclude, we reiterate that the overall system (inertial plus aerodynamic) is coupled and complex. A system of this complexity is very difficult to analyze in full generality, except through full simulation which makes the problem one of empirically validating guesses. To simplify the study of flight dynamics and control, a way is needed to uncouple the two systems. This can be achieved by modeling the aerodynamic forces and moments so that they depend on only a finite number of parameters, rather than on the entire motion history. The basic concepts underlying aerodynamic mathematical modeling are described in the companion paper to this one [1]. However, a realistic mathematical model cannot be achieved without a firm idea of the forms of nonlinear aerodynamic phenomena that need to be acknowledged within it. Nonlinear aerodynamics is the subject to which we now turn.

3. NONLINEAR AERODYNAMICS. In this section the fluid-dynamic phenomena that give rise to nonlinear aerodynamic forces and moments will be examined. A framework for classifying and studying these phenomena will be presented. The framework must be sufficiently broad to capture all essential features and thereby act as a guide in the mathematical

modeling of the aerodynamic forces and moments for flight dynamics analysis and simulation. The framework will consist of both an observational component and a complementary mathematical component.

First, however, we give a brief description of a simple aerodynamic flow problem that illustrates some of the important flow phenomena from which the resulting nonlinear aerodynamic forces and moments originate. The flow considered is that about a pointed body of revolution with a tangent-ogive tip. As shown in Fig. 3, the body is immersed in a water tunnel and dye is injected at various points along the side meridians [2]. In the upper left ($\alpha = 25°$), alternating colors of dye have been injected into the surface flow on the facing meridian. The dye streaks lift off the surface and roll up around each other to form a vortical structure as they move downstream. A similar mirror-symmetric pattern forms on the opposite side. This is the classic three-dimensional separation and roll-up into a pair of symmetrical vortices that occurs on all pointed slender bodies and delta wings at low to moderate angles of attack. At lower angles of attack (not shown) the dye streaks would remain in the viscous layer near the surface. They would flow around the body while moving downstream and pass off the rear of the body. For a blunt-based body this would also be a separation, but would not yield the strong streamwise vortices evident in Fig. 3. As the angle of attack is increased to 48° (upper right photo), a new flow structure is observed. Note now that dyes of different color have been injected along opposite meridians (light on facing meridian, dark in background). Near the rear of the body, the streaks of dye have collected to form sets of alternate colors (starting from the top they are dark, light, dark, light, dark, light).

The dark ones are difficult to see in photographic reproductions. The vortex structure has become asymmetric but steady (even at the nose) and departs rapidly from the body, while new vortices appear underneath. This is again a well-recognized flow structure on slender bodies and wings. It is important to note that a steady asymmetric pattern occurs, even though both the body and the boundary conditions are axially symmetric. At somewhat higher angles of attack ($\alpha = 60°$) we see another change in the flow structure. Although the flow pattern near the nose still appears to be asymmetric and steady, the flow in the wake is unsteady (smearing or apparent breaking of dye streaks). The pattern is more evident at $\alpha = 90°$ where a well-defined periodic shedding of dye is observed with considerable smearing of dye streaks (some chaotic structure) far in the wake. This is the classic periodic Karman vortex street observed in the wake of circular cylinders in crossflow.

The variation with angle of attack of the normal-force coefficient (directed normal to the body axis and in the plane of the angle of attack) that occurs on a similar body tested in a wind tunnel at various Reynolds numbers is shown in Fig. 4 (from [3]). The progression of flow structures is indicated across the bottom of the figure. Exact points where the flow structures change are not indicated, for they depend on Reynolds number. The normal-force coefficients shown represent mean values when unsteady phenomena occur. The type of unsteadiness, whether periodic or chaotic (aperiodic), is indicated at the right and is based on measurements on two-dimensional circular cylinders in crossflow [4]. The uppermost curve ($R = 0.35 \times 10^6$) is very similar to that which would be measured on the body illustrated in Fig. 3. The normal-force

coefficient at very low angles of attack (vortex-free flow or attached flow) changes linearly and very slowly with increasing angle of attack.

At the onset of separation and the appearance of symmetric vortices, the normal-force coefficient becomes a nonlinear function of angle of attack. These two flow regimes and the resulting normal forces are fairly independent of Reynolds number. However, at higher angles of attack (above 25°), where steady asymmetric vortex structures arise, Reynolds number begins to play an important role, and the nonlinearities become more exaggerated. It should also be noted that the onset of asymmetric flow also marks the onset of a side force normal to the plane of the angle of attack (not shown). It is easier to understand the effect of Reynolds number by examining the forces at an angle of attack of 90°. At $\alpha = 90°$, the variation of mean normal-force coefficient with Reynolds number is essentially the same as that observed on two-dimensional circular cylinders in crossflow. For $R = 0.35 \times 10^6$, the boundary-layer flow on the body is laminar, and separation occurs at or forward of the side meridians, resulting in a near-maximum value of the mean normal force. At this condition there is a very pronounced periodic vortex shedding in the wake and a large-amplitude periodic force component in both the normal and side directions. As the Reynolds number is increased, the wake flow becomes turbulent, with the turbulence moving forward in the wake toward the separation points. Associated with this, the separation points move rearward, the mean value of the normal force decreases rapidly, and the periodic nature of the wake structure and unsteady forces is replaced by a chaotic (turbulent) behavior with much smaller amplitude. As the Reynolds number is increased further, beyond

$Re \approx 1 \times 10^6$, the mean value of the normal-force coefficient begins to increase again and periodicity begins to reassert itself. Under these conditions, the small-scale turbulence has moved ahead of the separation points. At intermediate values of the angle of attack ($35° < \alpha < 60°$), we see a very strong interaction of a periodic to chaotic wake structure with the steady asymmetric vortex flow from the body. This brief description of flow over pointed bodies of revolution gives some idea of the flow's complexity, but also of its ordered nature. Additional flow structures resulting in important nonlinearities will be described in subsequent subsections.

3.1 A Framework. The description of the flow about the pointed body of revolution shown in Fig. 3 illustrates four essential elements of fluid flows. The four elements can be used to form an observational framework for the organization and study of aerodynamic flows. We associate the first element with the fact that the flows have definite structure. In the case shown in Fig. 3, the flow over the body separated from the sides, and the sheets of separated flow (flow with vorticity) rolled up to form vortices in different steady or unsteady configurations. We associate the second element with the fact that the structures change in systematic ways as parameters are varied systematically. In the case shown in Figs. 3 and 4, changes in two parameters, namely, angle of attack and Reynolds number, resulted in several changes in structure. The third element is in reality associated with structure, but its importance in aerodynamics and its seemingly incomprehensible nature sets it apart; it is chaos or turbulence. In Fig. 3, we saw the flow change through a series of well-defined steady structures to a periodic flow

structure and finally to chaotic flow. The fourth and final element is associated with the scale of the structures we observe. In Fig. 3 we were able to see only one or two scales. However, other scales, such as boundary-layer thickness, were present but were not detectable with the mode of observation used. The presence of small-scale phenomena or turbulence interacting with large-scale separated structures accounts for the rapid reduction in normal-force coefficient with Reynolds number increase at $\alpha = 90°$ in Fig. 4. The four elements — structure, change, chaos, and scale — would provide no more than a taxonomy for organizing fluid-flow information if there were not also a mathematical component to complement the observational one. We now consider the complementary mathematical framework.

A mathematical framework is required to provide a rigorous and systematic backbone to the observational material that is available in the study of fluid flows. The structure of fluid flows can be described by means of the topology of critical (singular) points of the flow. Research in this direction was originated in the 1950s by Legendre in France [5,6] and has been pursued by several other research groups in Europe and in the United States (e.g., [7-9]). Changes in the flow structures can be described in the context of bifurcation theory. Bifurcation theory has been used extensively in the study of several bounded fluid-flow problems (e.g., [10]). Recently, some of the concepts involved have been used to describe changes in external aerodynamic flows, principally by Tobak and Peake (e.g., [8]). As noted in the discussion of the observational framework, some changes (bifurcations) lead to chaotic or turbulent flows, and indeed it is known that bifurcation in even

simple systems can lead to bounded aperiodic solutions which, although deterministic, have chaotic properties that are similar to those of turbulence. This special class of chaotic solutions (structures) is characterized by the existence of what have been called strange attractors. Strange-attractor behavior as a possible property of turbulence will be discussed. Some of the properties of turbulence will also be described by means of the idea of fractals, an idea which in a sense describes a property of a strange attractor. The strange-attractor behavior was first reported by the meteorologist Lorenz [11] and was first posed as a model for turbulence by Ruelle and Takens [12]. The fractal properties of turbulence have been put forward by Mandelbrot (e.g., [13]). Finally, the scales of the flow structures will be discussed in the context of some group theory ideas. Many of the scaling concepts, such as dimensional analysis [14], and similarity exemplified in the description of the Blasius laminar boundary layer (e.g., [15]), are group properties of the equations describing the corresponding fluid flows and have been extant for many years.

In the following four subsections, each of the four elements of the observational and mathematical framework is described. Each subsection, with the exception of that concerned with chaos, begins with a description of the underlying mathematical ideas. These mathematical concepts are then related to the observations. However, because of the nature of chaos and our poorer understanding of its character, that section starts with a description of the observations and their importance to aerodynamics. As noted in the Introduction, the mathematical descriptions

that will be given are intended to be descriptive rather than rigorous, to illustrate possibilities and directions for research.

3.2 Structure: The Topology of Critical Points. The point of view taken here is that the important features of fluid flows can be described by a finite number of critical (singular) points which must conform to summation rules. The application of the topology of critical points in fluid flows was first introduced systematically by Legendre [5] in the mid-1950s and has been pursued extensively in recent years by several groups of investigators (e.g., [7-9]). We confine our discussion to flows that are steady in the mean and, in the following, to two-dimensional sections of the steady three-dimensional flow field. On any such section, a critical point is a point (x_o, y_o) where the velocity in the section is zero, that is,

$$\frac{dx}{dt} = u(x_o,y_o) = 0 \ , \qquad \frac{dy}{dt} = v(x_o,y_o) = 0 \ . \tag{3.1}$$

If we now expand the velocity (u,v) about the critical point (x_o,y_o) and retain only first-order terms, we get the following:

$$u = ax + by = 0 \quad \text{and} \quad v = cx + dy = 0 \ , \tag{3.2}$$

where, note, x_o and y_o have been taken as zero (by an appropriate translation of axes if necessary). A perturbation analysis about this point $(x_o = 0, y_o = 0)$ yields the structure of the local flow, that is,

$$\Gamma^2 + TR\cdot\Gamma + DET = 0 \ , \quad \text{where} \quad TR = a + b \quad \text{and} \quad DET = ad - bc \ . \tag{3.3}$$

The nature of the eigenvalues (Γ) yields the nature of the local flow structure. The various possibilities are shown in Fig. 5. When the eigenvalues are both real but of opposite sign (DET < 0), the flow structure contains a saddle point. When the eigenvalues are both real and of the same sign (DET > 0), the flow feature is a regular node. In the skin-friction line pattern on the surface, a regular node represents a point of attachment (TR < 0) or a point of separation (TR > 0). If the eigenvalues are complex, spiral nodes result, or in the pure imaginary case, centers result. Spiral nodes or centers usually signal the presence of vortices in the flow. When a critical point in a section is adjacent to a solid surface it will be one-sided (saddles and regular nodes only) and will be called a half-saddle or half-node.

When several isolated critical points occur in a flow section or in the skin-friction line pattern on a body, the assumption of a continuous vector field requires that they conform to topological summation rules. There are three surfaces on which these summation rules governing the collection of isolated critical points are of particular interest. The first is the surface of a three-dimensional, simply connected solid body. Here the nodes (N) and saddles (S) in the skin-friction line pattern must add up as

$$\sum N - \sum S = 2 \ . \tag{3.4}$$

This is the classic topology for bodies that can be formed from deformations of a sphere. The next surface of interest is that of a solid body mounted on the wall of a wind tunnel. Since the wind tunnel can be considered as a closed torus (the body mounted on the wall does not change the topological class) the summation rule is

$$\sum N - \sum S = 0 \ . \tag{3.5}$$

The final surface of interest is a plane that cuts a solid three-dimensional body. Here nodes and saddles occur both in the flow and on the intersection with the surface where they are half-nodes or half-saddles. This plane belongs to the class of topological surfaces formed from a torus with a spoke across the hole. The summation rule that applies here is

$$\sum N + \frac{1}{2} \sum N' - \sum S - \frac{1}{2} \sum S' = -1 \ . \tag{3.6}$$

Here the primed quantities denote half-nodes and half-saddles. These rules were put forward for studying fluid flows by Hunt et al. [7].

The richness of structures in fluid flows is well-illustrated in Van Dyke's book [16]. Additional examples are shown in Figs. 3 and 6 [17]. Both are separated flows on pointed bodies of revolution: one at subsonic speed (Fig. 3) and one at supersonic speed (Fig. 6). With the exception of the shock waves present in Fig. 6, the flow is topologically equivalent to that in the upper left photograph in Fig. 3 ($\alpha = 25°$). Leaving aside secondary structures (see below), if one were to construct the flow topologies that occur in a crossflow plane on a pointed body at various increasing angles of attack, one would get those shown in Fig. 7. The summation rule for the topology of the flow in a crossflow plane cutting a three-dimensional body is Eq. (3.6). The count of N, N', S, and S' is given in the figure. In the vortex-free flow, the flow in the section attaches at a half-saddle in front (windward) and leaves the body at the rear at a half-saddle. Thus, we have minus one for the summation rule. The next topological structure that occurs is the symmetric vortex flow (Fig. 7). Here the flow again attaches at a half-saddle as before,

but the rear flow is much more complex. The flow in the crossflow plane separates from the sides at half-saddles and the separated "sheets" roll up to form spiral nodes on each side. The flow at the rear is now directed back toward the surface and attaches at a half-saddle. To complete the topology and get the proper flow direction downstream a saddle that closes the flow structure is required. Again, the summation rule is satisfied. The third structure, first occurrence of the asymmetric vortex flow (Fig. 7), has the same topology as the symmetric case. The final structure shown in Fig. 7 is a three-vortex asymmetric configuration. This probably occurs with the development of a pair of critical points in the flow (a spiral node and saddle) on or very near the elongated separation sheet near the half-saddle point of separation. Additional asymmetric configurations occur that have more spiral nodes on alternate sides (not shown). Actually, a complete representation of the flow structures would require the inclusion of secondary vortices (with corresponding separation and reattachment points) that are in fact induced by the large primary vortices. Including them would have resulted in undue complexity for illustrating the basic point, although the secondary vortices may be at least partially responsible for setting up conditions for the creation of the new spiral node – saddle pair in the three-or-more asymmetric vortex configurations. We caution that although the summation rules provide necessary conditions for determining the structures, they are not sufficient conditions, and indeed, given the same number and types of critical points, the structures could be constructed in other ways. It is rather by studying the evolution of the structures and insisting that

particle paths (streamlines) remain continuous that one can be reasonably sure of constructing a "correct" sequence of structures.

Another example of fluid-flow structures is the surface oil-flow pattern (skin-friction lines) on a wing attached to a wind-tunnel wall and tested at transonic speeds (see Fig. 8; courtesy of Earl Keener, NASA Ames Research Center). A complete topological analysis has not been carried out as yet for this body. However, two points can be made. First, at $M = 0.90$ the flow has separated from the wing in the form of two spiral nodes, the origins of which are clearly illustrated in the oil flow. Saddle points are also clearly present. Second, here we see evidence of another parameter, Mach number, playing a role in causing flow structures to change; at $M = 0.82$, the flow is attached, evidenced by the smooth streamwise directions of the oil-flow lines. On the other hand, at $M = 0.9$ the flow is separated as indicated by the spiral nodes.

In concluding this section, three points must be made. First, the flow structures constructed with isolated critical points agree very well with observed flow structures in practical aerodynamic flows. Second, the topology of the critical points has proved to be a very useful tool in analyzing observational data or data obtained from computer simulations of the flows. Third, there are several important issues concerning three-dimensional flow separation to which topology may help provide answers. These issues include (1) the nature of three-dimensional flow separation and (2) the issue of open versus closed flow separation (e.g., [18]). Some of these issues may also require information concerning how flow structures change, the topic to which we now turn.

3.3 Change in Structure: Bifurcation Theory. Generally speaking, bifurcation theory is a theory of equilibrium solutions of nonlinear equations. In fluid-dynamic applications, we are interested in equilibrium solutions of evolution equations of the form

$$\vec{U}_t = H(\vec{U},\lambda) \ , \tag{3.7}$$

where $\vec{U}$ is the velocity vector and λ is a parameter (e.g., Reynolds number, angle of attack, Mach number). Equation (3.7) is sufficiently general (with dependence on the spatial coordinates understood) to include any of the forms of the equations said to govern fluid flows, for example, the Navier-Stokes equations. By an equilibrium solution of (3.7), we mean a solution to which $\vec{U}(t)$ evolves after the transient effects associated with the initial values have died away. Equilibrium solutions may be time-invariant, time-periodic, quasi-periodic, or chaotic, depending on conditions.

We are concerned with equilibrium solutions at two levels. The first occurs as a result of instability in (3.7). As the parameter λ is varied, a critical value λ_c can be reached beyond which the original solution becomes unstable. New solutions, called bifurcating solutions, appear, some of which may be stable and some unstable to small perturbations. By stable and unstable we mean the following: If a small perturbation of the solution decays to zero as $t \to \infty$, the solution is said to be asymptotically stable; if the perturbation grows, the solution is said to be (asymptotically) unstable. Stable branches of bifurcating solutions can be either local or global. A bifurcating solution is said to be local if it can be mapped onto the original solution without

cutting the solution space; if it cannot, the bifurcation solution is said to be global. In addition, the bifurcation can be supercritical or subcritical, as illustrated in Fig. 9. In a supercritical bifurcation (shown by the pitchfork bifurcation), there is at least one branch of stable bifurcating solutions that is continuous with the original solution at the bifurcation point λ_c. Thus, for a small change in λ across λ_c, there is a stable bifurcating solution that is $0(\Delta)$ close to the original solution such that as $\lambda - \lambda_c \to 0$, $\Delta \to 0$. This is not the case for a subcritical bifurcation shown on the right of Fig. 9. Here, for a small change in λ across λ_c, there is no branch of <u>stable</u> bifurcating solutions that is continuous with the original branch. This type of bifurcation normally leads to hysteresis behavior because the critical point for the upper branch in the case shown does not occur at the same value of λ_c as it does for the lower branch. The symmetrical bifurcation curves shown in Fig. 9 are often the result of an idealized problem. In practice there is less enforced symmetry, or there is a boundary condition or a scale that was suppressed in the idealized problem. When these are brought into consideration, the idealized bifurcation diagram may undergo an <u>unfolding</u>. This is illustrated in Fig. 9 with the pitchfork. The idealized pitchfork has the following form (to leading order)

$$\psi^3 - \lambda\psi = \psi(\psi^2 - \lambda) = 0 \ , \tag{3.8}$$

whereas the general (unfolded) bifurcation to this order has the form

$$\psi^3 + a(\lambda)\psi^2 + b(\lambda)\psi + c(\lambda) = 0 \ . \tag{3.9}$$

For the case shown in Fig. 9, $a = 0$, and b represents the effect of a small imperfection. Bifurcation in the case of Couette flow between

rotating cylinders (the Taylor vortex problem) has this form, in which the c term is the result of including ends in the concentric cylinders rather than treating the idealized problem in which the ends are at plus and minus infinity. The first stage of the Taylor vortex problem typifies a common type of bifurcation in which an original time-invariant equilibrium solution is replaced at the bifurcation point by another time-invariant equilibrium solution, in this case one describing the Taylor vortices. A second type of bifurcation is the "Hopf" bifurcation in which the original time-invariant equilibrium solution is replaced by a branch of stable equilibrium solutions which are time-periodic. In turn, time-periodic solutions can bifurcate into quasi-periodic solutions. The Hopf-type of bifurcation is common in aerodynamics. An example is the Karman vortex street in the wake behind a circular cylinder for $Re > Re_c \approx 50$. A third type of bifurcation of great interest occurs when a quasi-periodic equilibrium solution is replaced by a bounded aperiodic solution having chaotic properties. Solutions of this kind, of course, recall the turbulent-like behavior typical of flows at high Reynolds numbers.

The second level at which we have a particular concern with equilibrium solutions focuses on the class of equilibrium solutions that is time-invariant. Here, we concentrate attention on the critical points in the equilibrium flows where $\vec{U} \equiv 0$. With $\vec{U}_t \equiv 0$ in (3.7), we can recast (3.7) to directly describe particle trajectories or streamlines:

$$\vec{U} = \vec{X}_t = G(\vec{X},\lambda) \ , \tag{3.10}$$

where $\vec{X}$ is the spatial coordinate of the fluid element. Equation (3.10) in effect governs the flow structures that we studied earlier in Sec. 3.2. Here, as λ crosses λ_c, a critical point may bifurcate into multiple critical points, or a new pair of critical points may appear, or a pair disappear. However, bifurcation at this level need not imply nonuniqueness in the governing flow equations. Equilibrium solutions may remain stable and unique on either side of λ_c. The bifurcation of critical points in the flow will be referred to as structural bifurcation. All structural bifurcations are global in the mapping sense described earlier. That structural bifurcations are unique appears to be the case in computations based on the incompressible Navier-Stokes equations for the onset of steady separated flow behind a two-dimensional circular cylinder as the parameter Reynolds number (Re) increases past a value of 7. For $Re < 7$ the equilibrium solution indicates attached flow and is unique; for $Re > 7$ the equilibrium solution indicates separated flow and appears to be unique. The latter conclusion is based on the observation that flow structures develop smoothly through $Re = 7$, with no indication of the possible existence of multiple solutions. However, as Re passes through 7, the rear stagnation point (half-saddle) splits, yielding two centers, three half-saddles, and a saddle to form the symmetric separation region.

The general topic of bifurcation theory has received considerable attention in the past few years with development of an extensive body of literature. When the focus is purely on the classes of steady-state solutions of a governing evolution equation it is often termed catastrophe theory, after the work of Thom [19]. Several examples of this genre of

work are given in [20-23]. An example of extensive use of bifurcation theory in a fluid mechanics setting is presented in [10].

Consider now some examples of changes of flow fields that illustrate these various bifurcations and their various properties (local versus global; supercritical versus subcritical; periodic and aperiodic). The first is that of flow about a body of revolution which we have already introduced. The principal changes in the flow structures observed in the crossflow plane with increasing angle of attack are shown in Fig. 10. The change from vortex-free (attached) flow to symmetric vortex flow is an example of a structural bifurcation in the topology which occurs at a critical value of angle of attack, but flows both before and after the change are believed to be unique. In the crossflow plane, the structural bifurcation is global, in that one flow field cannot be mapped to the other without cutting the field. The next change with angle of attack, from symmetric to asymmetric vortex flow, is a true bifurcation because both solutions exist beyond a critical angle of attack, but only the asymmetric one is stable. It has two mirror-symmetric configurations. This bifurcation is believed to be supercritical, but in the mapping sense it is local in that a simple stretching of the field would turn the symmetric flow into an asymmetric flow. With further increases in angle of attack, the next change in the sequence of flows is again asymmetric, but new spiral nodes and saddles appear in the crossflow plane. This again is a structural bifurcation. Finally, at very high angles of attack, the bifurcation is normally of the Hopf type, giving rise to periodic wake-like flow. However, under certain conditions,

the periodic wake-like flow changes quickly to an aperiodic flow. These conditions are associated with another parameter, namely, the Reynolds number.

The second example concerns asymmetric vortex breakdown on a very slender delta wing. Vortex breakdown occurs along the core of a vortex when the axial flow undergoes a rapid deceleration, causing the core of the vortex to increase in size rapidly, as shown in Fig. 11 (from [24]). The phenomenon has been studied extensively (e.g., [25-26]). Here, we will be concerned with the special condition when the pair of leading-edge vortices on the delta wing break down and there is a mutual interaction. The phenomenon, which occurs principally on very slender delta wings, was first observed by Lowson [27]. It is illustrated in the form of a bifurcation diagram in Fig. 12, where the ordinate Δ represents chordwise distance between the origins of the two breakdowns. Lowson noted that at low angles of attack (roll angle $\psi = 0$) the breakdowns occurred symmetrically. Thus, $\Delta = 0$, as shown in Fig. 12. Beyond some angle of attack $\alpha > \alpha_c$ there occurred a finite asymmetry in the positions of the vortex-breakdown origins ($\Delta \neq 0$). Continued increases in α resulted in increases in Δ. However, when α was decreased, the return to $\Delta = 0$ (the symmetric configuration) occurred at a value of α smaller than α_c. Thus, as illustrated in Fig. 12, we have a source of hysteresis. Note that Δ has two branches in view of the existence of mirror-symmetric solutions. The asymmetric vortex breakdown gives rise to an aerodynamic rolling moment C_ℓ that is proportional to the magnitude of Δ. Now, let the angle of attack α be fixed at α_1. Increasing the roll angle ψ in one direction increases Δ, and increasing ψ in the

opposite direction diminishes Δ and proportionately C_ℓ, as shown. At some negative value of ψ, flow conditions favorable to vortex breakdown in the opposite direction force the breakdown positions to switch directions. With this we see another source of hysteresis. Thus, we have complex bifurcations dependent on two parameters, α and ψ. The solution surface has the form of cusp catastrophe surface.

The third and final example again involves hysteresis. Figure 13 [28] shows the side forces generated on the nose of a body which is at 90° angle of attack and is rotating about the velocity vector with angular velocity ω (see the inset in the upper left-hand corner of Fig. 13). The body nose has a square cross section with rounded corners. When the Reynolds number is large and the flow in the boundary layer over the body is turbulent, rotation of the body creates a side force C_Y opposite to that of the spin (antispin). The flow is attached to the sides of the body, and there is a turbulent (chaotic) wake as shown schematically in the lower right-hand sketch in Fig. 13. This chaotic flow in the wake gives rise to a small chaotic side force which generally is not of great concern. For low-Reynolds-number conditions, the boundary-layer flow on the body is laminar, giving rise to a much different flow, and hence to a side force, as indicated by the curve marked by circles in Fig. 13. At low reduced spin rates (Ω), the flow separates from both sides of the body (not sketched) and we get a large periodic side force (also not shown) with a small mean side force that increases slowly with Ω until a value of Ω is reached at which the flow attaches to the body on the side toward which it is spinning (see upper right-hand sketch in Fig. 13), with a resulting large increase in side

force. Further increases in Ω cause small reductions in side force. The bifurcation that occurs here would appear to be supercritical, but very rapid (no hysteresis is observed). However, at intermediate Reynolds numbers and low spin rates we get either the flow attached to both sides or to one of the two sides depending on the direction of spin and whether spin rate is increasing or decreasing. In these circumstances a hysteresis results, as shown in Fig. 13; for example, at $Re = 0.5 \times 10^6$.

As can be seen from the three examples presented, there are many types of bifurcation that occur in practical aerodynamic flows. Furthermore, these bifurcations have significant ramifications for flight dynamics. They must be understood if logically consistent models of the aerodynamics are to be formulated.

3.4 Chaos — Strange Attractors and Fractals. Turbulent or chaotic flow plays a very important role in aerodynamics but is not fully understood. In addition, our present understanding of how strange attractors and fractal properties are related to turbulence is less well advanced than is our understanding of how critical points in the flow topology and bifurcation theory are related to the origin and change of flow structures. For that reason, this section will start with the observational framework; then the mathematical concepts will be introduced.

All fluid flows suffer chaotic behavior at sufficiently high values of Reynolds number. This basic property of fluid flows appears to be modeled by the Navier-Stokes equations, which are said to govern the flows, through the mechanism of multiple instabilities. On walls, turbulent (chaotic) behavior normally first occurs in the boundary layer,

and in free shear layers it occurs downstream of vorticity-producing surfaces. An example of a turbulent boundary layer is shown in the photograph in Fig. 14 [29]. The small-scale turbulence near the wall (scales are of the order of the boundary-layer thickness or smaller) gives rise to turbulent momentum transport and a significant increase in the mean (time-averaged) drag force on the body. There are other small-amplitude, high-frequency unsteady forces but these generally are not important. (They may be important for sound generation or in certain structural fatigue problems.) In some cases the small-amplitude, small-scale turbulence can interact with other larger flow structures to significantly alter the aerodynamics. Finally, there are some large-scale chaotic-like flows that can occur, for example, during the stall of a wing under some Reynolds-number conditions. The state of understanding of any of these chaotic flows is rather limited. Ideas from bifurcation theory that have drawn attention to the behavior of strange attractors already have had a significant effect on our understanding of the transition from laminar to turbulent flow. The classic view of transition due to Landau [30], that of an infinite set of bifurcations occurring which completely fills out the wave-number space, has not corresponded to observations in which there appeared to be a finite and small number of bifurcations ending in a chaotic flow. With the discovery that even relatively simple deterministic differential equations could yield bounded aperiodic solutions with chaotic-like behavior, a route to turbulence consistent with observations became available, entailing a finite number of bifurcations ending with bifurcation to a strange attractor. This was first proposed as a model for transition by Ruelle and Takens

in 1971 [12]. Since then, others have proposed similar routes to turbulence via strange-attractor behavior. A recent review of the various scenarios is given by Eckmann [31]. Given the role played by the strange attractor in transition, it is logical to ask about its properties and whether it plays a role in fully developed turbulence. These are questions to which we now turn.

Strange attractors can occur in forced dissipative systems with relatively small nonlinearities. A strange attractor can be loosely defined as a subset of solutions all of which are bounded and aperiodic. Each member of this bounded and aperiodic set occupies zero volume in the solution space. That is, for example, if the solution is a trajectory (dimension-one) in a plane (dimension-two), the trajectory, although staying within a bounded region of the plane, never occupies any area of the plane. This gives rise to the fractal property of the strange attractor, to which we will return later. The strange attractors are also sensitive to initial conditions. Behavior of a system containing a strange attractor that was first discovered by Lorenz [11] is shown in Fig. 15. Since its discovery, the system has been studied extensively by many authors (e.g., [32]). The equations for the system are

$$\frac{dx}{dt} = \sigma(y - x) ,$$

$$\frac{dy}{dt} = -xy + Rx - y , \qquad (3.11)$$

and

$$\frac{dz}{dt} = xy - Bz ,$$

where σ, R, and B are system parameters. There are several aspects of the behavior illustrated in Fig. 15 that are similar to turbulence.

First, although the solutions are deterministic there is chaotic-like behavior, but there is also an overall structure. It is conjectured here that the turbulent streaks that are observed in both experiments and computations of plane flows have a structure that is suggestive of strange-attractor behavior. They are not stationary in flows but rather tend to wander with time, all the while retaining the same basic structure. Figure 16 is an example of these structures taken from the computation of a turbulent channel flow carried out by Moin and Kim [33]. Shown are velocity contours at an instant in time in a plane parallel to the channel wall. The elongated structures (streaks) move around with time in an erratic manner. The second important characteristic of a strange attractor that is similar to turbulence is a result of the fact that the bounded aperiodic solution does not fill the solution space, as noted earlier. This gives rise to intermittency. For example, a measurement probe traversing through the plane of the strange attractor illustrated in Fig. 15 would record an intermittent series of pulses on crossing different segments of the trajectory. A review of the relationship of strange attractors to turbulence is given by Lanford [34] while Ott [35] reviews the role of strange attractors in chaotic dynamical systems.

It is intermittency which leads to fractal properties (e.g., [13]). To understand fractal properties we will first consider fractal curves. A fractal is a curve that is everywhere continuous but nowhere differentiable. A simple example of this is the Koch curve shown in Fig. 17. The curve is constructed by the following recursive procedure: Take a line one unit long and divide it into three equal segments. Remove the

center segment and replace it with two equal segments to form a hat (see Fig. 17). This process is repeated recursively on each of new segments that are formed at successive steps. Now the length of the resulting curve increases without limit as the number of repetitions (n) increases without limit, but the curve does not fill up any space. Only a line with apparent texture results. The following question arises: Is there a way to form a relationship between the line length and the unit of size at any point in the iteration? There is, and it is shown by the equation,

$$L = s^{\mu} , \tag{3.12}$$

where L is the length of the line and s is the length of the element used to construct L. Hence, for the Koch curve we have

$$\left(\frac{4}{3}\right)^n = \left[\left(\frac{1}{3}\right)^n\right]^{\mu}$$

or

$$\mu = 1 - \frac{\ell n\ 4}{\ell n\ 3}$$

Now μ can be interpreted as the difference between the Euler dimension (D_E) of the element (s), which in this case is 1, and the dimension of the line L, which is called the Hausdorf dimension (D_H). Hence

$$\mu = D_E - D_H ,$$

or, for the Koch curve, $D_H = \ell n\ 4/\ell n\ 3$, which is about 1.28. Note that if $D_H = D_E$, the length of the line does not depend on the size of the unit of construction which is what one expects for smooth curves.

A better example and one more closely related to turbulence is the second example in Fig. 17, namely, that of a surface. One may think of this surface as a surface of vorticity. It is distorted in a recursive manner as follows. Divide the unit square into nine smaller squares. Now remove the four corner squares and the center square and replace them by building a small square box over the open squares (center box down for convenience). Now with each of the 29 sides of the new figure, repeat the process. This surface becomes more and more distorted with each step, and the actual surface area increases without limit as the number of iterations (n) increases. Hence this surface in two dimensions becomes more and more distorted but never fills up space in three dimensions. In a manner similar to that used for the Koch curve, the Hausdorf dimension is found to be $\ell n\ 29/\ell n\ 9 + 1$ or about 2.54. Now this is a rather simplistic model for a sheet of vorticity that has been distorted into a parcel of turbulence because of instabilities. Even though the model is simplistic, it is true that a hot wire passing the distorted sheet would exhibit intermittency. Observations that high-Reynolds-number turbulent flows exhibit intermittency go back to a paper by Batchelor and Townsend [36]. Those authors noted that in high-Reynolds-number homogeneous turbulent flows, the vorticity was not distributed uniformly but was concentrated on sheets or other localized regions of space. Atempts have been made to derive a Hausdorf dimension for this turbulence based on higher-order statistical information. Values between 2.0 and 3.0 have been derived. However, the reduction of information on the higher-order statistics to a Hausdorf dimension requires specification of a topological form of the turbulence, and this step has led to

considerable disagreement. Mandelbrot [13] suggests that reasonable topologies bound the value of the Hausdorf dimension between 2.5 and 2.7. In a recent attempt to establish a basis for these values, Chorin [37] calculated the distortion of a vortex tube using the Euler equations. That calculation showed that the vorticity contracted (in an L_2 norm sense) to a Hausdorf dimension of about 2.5, in reasonable agreement with the lower bound postulated by Mandelbrot.

3.5 Scale: Group Theory. In all flows, and with bifurcations of the flow structures, a broad range of both spatial and temporal scales can occur. The scales are normally determined by the interaction between the various physical effects that come into play. For the sake of simplicity, the discussion will concentrate on four basic ideas and relationships that are of special importance. The first is dimensional analysis, which is widely used. It provides relationships between important physical effects such as those between inertial and viscous effects. A simple example of dimensional analysis is the derivation of the form of the drag force on a flat plate in uniform flow. The drag can be written functionally as

Drag (D) = F [velocity (V), density (ρ), length (L), fluid viscosity (μ)]. (3.13)

Since D, V, L, and μ have dimensions composed of mass, length, and time, the equation for drag can be rewritten, using Buckingham's pi theorem [14],

$$C_D \equiv \frac{D}{\rho V^2 L} = G\left(Re = \frac{\rho VL}{\mu}\right) . \qquad (3.14)$$

Here the Reynolds number Re can be interpreted as the ratio of an inertial property, the length L, to a length characteristic of the viscous flow, namely, $\mu/\rho V$. We know from experience that there still remains much richness to this problem in that there are many structures with various scales that develop with different values of Re, in particular turbulence.

The second class of relationships or scales concerns those scaling properties that occur within a given class of flow structure. Again we can use the flow over a flat plate as an example, but now restrict ourselves to a Reynolds number for which the flow remains laminar. An examination of terms in the full fluid-flow equations on the basis of Re (ratio of plate length to viscous scale) being of the order of 10^5 (laminar flow) indicates that several terms are of second order. In fact, the entire momentum equation normal to the plate becomes of second order. Retaining only first-order terms yields a much simpler form of the equations, with Reynolds number as the parameter. It can be quickly shown that this reduced equation has a self-similar form [15] if all dependent and independent variables are normalized by their counterparts (e.g., velocities by free-stream values of velocity and longitudinal distance by the plate length) with the exception of the vertical distance y which is normalized as

$$\bar{y} = \frac{y}{x} (Re)^{1/2} , \tag{3.15}$$

where $Re = \rho V x/\mu$ is the local Reynolds number. This normalization collapses all of the laminar flow solutions (where $10^5 > R >> 1$) to a single solution. We have a continuous scaling within a given class.

The next logical step in considering scales would be to consider problems with two scales and their interactions. Here, we consider two examples. The first involves the merging of critical points (three critical points), shown schematically in Fig. 18. At fine resolution we distinguish two saddle points with a node located between them; however, as the resolution decreases the structure is recognized only as a single saddle point. One can now ask whether it is essential to resolve the three critical points to get an overall correct solution. This is a very important issue for finite-difference computational methods because the need to resolve closely spaced critical points can markedly increase the grid size required to obtain a valid solution. The answer may depend on the particular information required and how accurate it must be. If it is important to resolve the critical points, another problem arises: When the full fluid-dynamic equations are approximated, for example, by averaging, care must be exercised to ensure that the reduced equations are still able to capture the change (bifurcation) from the single saddle point to the two saddle-point-one node configuration given in this example.

A second example of multiple scales is illustrated in Fig. 19 which presents a photograph of flow normal to an airfoil, together with a schematic of the flow. The flow of particular note here is that emanating from the trailing edge [38]. The flow separates from the trailing edge and rolls up into a large vortex (spiral node) structure. In addition, the separation layer (free shear layer) is itself breaking down into a series of spiral nodes separated by saddle points (not visible). This is a two-scale problem in which the two scales have different physical

origins. The large-scale vortex is a measure of the total vorticity in the sheet and is relatively insensitive to Reynolds number. The dominant scale here involves an overall dimension of the airfoil. The small vortices are due to a local instability of the free shear layer. Their scale is a function of the shear-layer thickness, and is thus sensitive to the Reynolds number. As a result, the large structure tends to dominate the flow, but under certain conditions the interaction can be important. Again, how much of this flow structure must be resolved influences not only the question of grid sizes in finite-difference computations, but the types of approximation that might be imposed on the equations to simplify them without losing the information that is essential.

Singular perturbation methods and the method of inner and outer expansions [39] can be used to treat some of these two-scale problems. These approaches are particularly applicable to merged singular-point problems. However, the problem involving interaction of the two scales, for example of the spiral nodes in Fig. 19, does not seem to be amenable to these approaches nor do there appear to be other methods available at present.

The fourth and final issue to be discussed regarding scale is that of the multiple scales inherent in turbulence. In many cases of interest the multiple scales that are present strongly influence the mean properties of the flow, but the details of all these scales are of relatively minor interest. For example, reconsidering the flat-plate boundary layer described earlier, but now at higher Reynolds numbers where the flow near the plate has become chaotic, we have many scales that have had a strong

influence on the mean velocity profile in the layer and hence on the drag. How do we develop a rational approach that will account for the integral effects of these scales without having to deal with all of the details? The classic approach is by analogy to the interactions of molecules in a gas in which an equation is developed for the transfer of momentum by means of a viscous term depending on the mean path length between molecular collisions. On this basis, an analogous model for turbulence was developed by Prandtl [40] in 1925. The appropriate length scales were understood to vary through the layer, because large scales could not exist near the wall. Empirical expressions developed for mixing lengths resulted in excellent predictions of mean profiles and drag [41]. However, these empirical expressions did not work well for other flow situations, in part because the concept contained an assumption concerning the distribution of scales under equilibrium conditions which was not universally true. Thus far it has not been found possible to replace the informal basis of the mixing-length idea by more formal and rigorous extensions. Extension by analogy to nonequilibrium chemistry has been proposed [42]; again however, there is no rigorous basis for this approach. Recent work in other areas of research, in particular phase transitions in condensed phase matter, holds considerable promise of providing a basis for the development of rational approaches to the fluid dynamics problem. This is the idea of the renormalized group that has been developed by Wilson and Kogut (e.g., [43]). Feigenbaum et al. [44], in particular, have adapted renormalized group ideas in a novel way that has called attention to the existence of "period-doubling" phenomena and scaling laws governed by "universal numbers." These ideas

are currently under rapid development in several directions [44, 45], and have the potential of describing not only alternative routes to turbulence but fully developed turbulence as well. Reviews of these developments, including their relevance to fluid dynamics questions are contained in [31], [35], and [46].

3.6 Aerodynamics with Unsteady Boundary Conditions. In all of the material covered so far in this section, the body has been assumed to be either rigidly fixed or stationary in some uniformly rotating coordinate system; that is, its shape and orientation have been assumed fixed relative to the oncoming wind. A few comments are in order for bodies that are free or forced to move relative to the wind. If this movement is slow relative to the time taken by a particle of fluid to move from the tip to the rear of the body, the previous discussions of structure, change, chaos, and scale will hold in general. The resulting flows will be the same as those for the steady cases, with the exception that they will be shifted slightly in phase relative to the motion. This phase shift can be expected to change slowly (linearly) with the rates within a given flow topology, but may shift rapidly when the flow topology changes. It should be noted, however, that there has not been a great deal of study relative to this latter point. For movement that occurs on the same order of time as flow over the body, there can be a very strong influence on the flow. One effect of such movement on the flow is illustrated in Fig. 20. Here we show flow visualization pictures (by means of hydrogen bubbles [47]) and lift coefficient (C_L) data [48] for an oscillating airfoil in what is referred to as dynamic stall. At the bottom of the figure are shown several plots of C_L versus α for

different values of $k = \omega c/2V$ where ω is the frequency, c is the chord, and V the free-stream velocity. This parameter represents the inverse of the chord lengths traveled per cycle; that is, for $k/\pi = 0.1$ the airfoil in free flight would travel forward 10 chord lengths while undergoing one cycle of oscillatory motion. Under static (nonoscillatory) conditions, the flow remains attached to the airfoil for angles of attack up to 12°, at which point the onset of flow separation causes the lift curve to break and finally to decrease rapidly. After separation, the flow tends to be periodic; that is, the evidence suggests that a Hopf bifurcation occurs at $\alpha \simeq 12°$. When k is small, we can hardly detect the difference in C_L (there is a slight change) between the static and oscillatory case, as long as we are below $\alpha = 12°$. However, beyond $\alpha \simeq 12°$, there are pronounced differences that increase drastically as k becomes larger. These differences also depend on whether the angle of attack is increasing or decreasing. The effect on the flow in a water tunnel is shown for $k = 0.25$ in the top part of Fig. 20. On the left, $\alpha = 15°$ on the part of the cycle in which α is increasing. The flow is generally attached or has a very thin separated layer with strong periodicity evident in the wake. On the right, the angle of attack is the same, but on the part of the cycle in which α is decreasing. Here we see a massive separation occurring in which there is considerable vortical structure that is not necessarily periodic. This class of flows is important for helicopters and high-performance aircraft, but is poorly understood. The root of the problem may reside in the fact that the airfoil oscillation is modulating, in some highly nonlinear manner, the periodic flow resulting from the Hopf bifurcation near $\alpha = 12°$.

3.7 Summary of Aerodynamic Behavior. The foregoing considerations would suggest at least six major subdivisions of the aerodynamic forces and moments. These are shown in Fig. 21. Figures 21a-21e deal strictly with forces on bodies moving at constant velocity and orientation. The type of bifurcation that can give rise to these characteristics is noted. The rate-dependent forces and moments also can be expected to change at these bifurcations. The sixth subdivision (Fig. 21f) is one in which there are strong rate-dependent effects. Very little is known at present of this latter category. Since, in general, aerodynamic forces and moments are functionals of the motion history, they could potentially depend on variables other than merely orientation (α) and rate ($\dot{\alpha}$). In principle, the dependence could rest on all of the history. To understand these issues better, a rational framework for creating a mathematical model of the aerodynamic forces and moments is required. Aerodynamic modeling is taken up in the companion paper to this one by Tobak et al. [1]. Assuming that a method for modeling is available, we now turn to the flight-dynamic behavior caused by some of these nonlinear aerodynamic forces and moments.

4. FLIGHT DYNAMIC BEHAVIOR. With a framework for understanding the aerodynamic flows and with rational mathematical models for the aerodynamic forces and moments (in part) in hand, our last step is to bring these results together with the inertial characteristics of the vehicle and to illustrate some of the flight-dynamic behavior that can result. Here again we shall be using much of the language that was used in Sec. 3, in particular that associated with the topology of critical points, bifurcation theory, and strange attractors; however, there is a difference

here in how these are to be viewed. In discussing the aerodynamic flows, we were dealing with a continuum and hence with partial differential equations. The topological structures discussed were "real" physical structures. In contrast, in the discussion to follow we deal with trajectories of an isolated solid body. In the main, the governing equations are ordinary differential equations, and the structures (critical points) are in the phase space of position and velocity. At any time, the body occupies only one point in this space, and hence the phase portrait describes all the possible states. The study of flight dynamic behavior has only recently been approached from the bifurcation theory standpoint (see e.g., [49, 50] and the paper by Hui and Tobak [51] in this collection).

The full description of the motion of a rigid body requires six degrees of freedom and hence can be very complex; illustrations of this order of complexity would not provide much insight. Therefore, with some exceptions to be noted, this section will be confined to the discussion of inertial systems having a single degree of freedom. The motions to be considered all will involve angular rates of change, which makes it convenient to define the relevant angular coordinate geometrically rather than kinematically as was done earlier. To mark the distinction, we designate the angle of attack by σ in place of α. Figure 22 lists the equations for a single-degree-of-freedom oscillatory system for five different levels of modeled aerodynamic contributions. In each case the aerodynamic mathematical model is underlined. In the last two cases, the aerodynamic contributions are left undetermined

because complete rational models have not yet been developed. Some of the flight-dynamic characteristics are also listed.

The single-degree-of-freedom system with aerodynamics linear in both σ and $\dot{\sigma}$ yields relatively simple flight dynamic characteristics. There is a single critical point at $\sigma = 0$. If B is negative, the system is called statically unstable, and the critical point can be either a saddle point or a node depending on the value of A. In the past, aircraft designs having negative values of B were avoided at all cost. Recent advances in control system hardware, coupled with significant potential increases in aircraft performance, have led to consideration of aircraft having negative static stability ($B < 0$). When B is positive, the system is statically stable, and the critical point is always a node. Depending on the value of A, the critical point can be a regular or spiral node, or, in the special case of $A = 0$, it can be a center. The system is said to be dynamically stable if $A > 0$, dynamically unstable if $A < 0$. The phase portrait for a statically and dynamically stable system is shown in the upper left of Fig. 23. This linear system is normally associated with low angles of attack σ. At higher angles of attack the aerodynamic contributions A and B become nonlinear in σ but, for slowly varying motions, the aerodynamic damping term continues to be linear in $\dot{\sigma}$. This is the case to which we now turn.

The most general nonlinear, single-degree-of-freedom case is governed by the Lienard equation and, depending on the nature of the nonlinearity, can have a single or multiple critical points. It can also have limit cycles which result from Hopf bifurcation from a stable critical point as well as super- and subcritical bifurcations. Two cases

are illustrated in Fig. 23. In the upper right is the case for a nonlinear $B(\sigma)$ which has only one stable critical point (i.e., $B(\sigma) > 0$ for $|\sigma| > 0$). But the values of $A(\sigma)$ are such that near the critical point ($\sigma = 0$) the solution is dynamically unstable ($A(\sigma) < 0$; $|\sigma| > 0$); that is, trajectories from the origin will spiral outward. On the other hand, far from the critical point the value of $A(\sigma)$ is such that the solution is dynamically stable ($A(\sigma) > 0$; $|\sigma| > 0$) and trajectories spiral inward. Dividing inward- and outward-directed spirals is a closed path in the $(\sigma,\dot{\sigma})$ plane to which all trajectories are attracted. Hence, limit-cycle motion occurs for all trajectories. The second case is illustrated on the lower left of Fig. 23. Here $A(\sigma) = 0$, and we have only nonlinear $B(\sigma)$ which in this case can be written as $B(\sigma) = B_0 + B_1\sigma^2$, where $B_0 < 0$ and $B_1 > 0$. Hence, the system is statically unstable for small values of σ but becomes statically stable for larger values of σ. The three critical points are $\sigma = 0$ (unstable), and $\sigma = \pm(-B_0/B_1)^{1/2}$ (stable). Since there is no damping, all trajectories are closed. There is a separatrix that divides trajectories that are closed about the origin (large amplitude) from those about the critical points $\sigma = \pm(-B_0/B_1)^{1/2}$. If $A(\sigma)$ is nonzero the variety of possible motions is large. In the lower right of Fig. 23 we have illustrated one possibility when nonlinear damping is added to the nonlinear static case just described. Here the system is undamped near the stable nodes $[\sigma = \pm(-B_0/B_1)^{1/2}]$ but damped far from these nodes. Hence, a stable limit cycle can develop around each of the two nodes, and also a limit cycle can occur that encloses all three nodes, as shown by the outer limit cycle in Fig. 23. As we have seen in Sec. 3, the aerodynamics can

change with various parameters in the system, and hence we can expect changes or bifurcations in the flight-dynamic behavior that are driven by nonlinear aerodynamics resulting from at most a supercritical bifurcation in the fluid flow. A complete description of this equation and its bifurcation structure can be found in [52].

The third case of interest is one with aerodynamic hysteresis. This is represented in equation form with the inclusion of a switch term (h) in A and B to indicate which branch is operative. Here again the types of behavior are many with the possibility of bounded aperiodic (strange attractor) solutions. The example to be considered here is one with two degrees of freedom; it is speculative in the sense that a full simulation of what is to be described has not been performed, but the ideas seem to be consistent. The case is patterned after the aerodynamics of the delta wing with asymmetric vortex breakdown described in Sec. 3.3, and the strange-attractor behavior described by Diener and Poston [53]. The example is illustrated in Fig. 24. The bivalued rolling moment (C_ℓ) variation with angle of attack (σ) (with the subcritical bifurcation omitted) is shown in the upper right. At an angle of attack σ_1 we have a rolling-moment curve C_ℓ versus roll angle (ψ), as shown on the left. It is required that an aerodynamic control surface produce a trim rolling moment as shown; that is, there is a stable trim (stable critical point) at ψ_1. Now the damping (rate-dependent) term is taken as nonlinear such as to produce a limit cycle about ψ_1. If the amplitude of the limit cycle were small the motion would always stay on the upper branch of the hysteresis curve. However, if the amplitude were large enough to pass the break point in the curve the motion would traverse

both curves. At this point the motion would be at least periodic (a limit cycle) or possibly that associated with the existence of a strange attractor. Motion corresponding to presence of a strange attractor is much more apt to occur if the body is also allowed to oscillate freely about σ_1 where the static pitching-moment curve is such that there is only one stable point (stable critical point) at σ_1, and the pitch-damping is such that a limit cycle in σ can occur about σ_1. Combining these two motions, assuming that inertial coupling between the modes is relatively small, we arrive at the motions shown on the lower part of Fig. 24. Here a C_ℓ surface versus σ and ψ is shown. It has a fold owing to the hysteresis (i.e., a cusp catastrophe). The trim point (σ_1,ψ_1) is on the upper sheet. When the limit-cycle amplitude does not exceed the distance to the fold, all trajectories inside the limit cycle converge to it. Those outside either converge to it or some of those that start out or get to the lower surface can be injected back into the upper sheet inside the limit cycle and hence converge from inside. This is the case on the lower left. Now, if the limit cycle amplitude is large enough to cross the fold, trajectories inside the limit cycle spiral out to fall off the upper sheet onto the lower sheet only to be reinjected back into the limit cycle on the upper sheet. This, it is believed, will lead to behavior corresponding to presence of a strange attractor. The motion is definitely bounded. Whether it is aperiodic needs to be checked.

The one-degree-of-freedom cases with periodic or bounded aperiodic aerodynamic forces noted in Fig. 22 are very poorly understood. It is known that they are associated with dynamic stall, "lock in" (a resonant

condition), and buffeting. Much remains to be done here, but first reasonable mathematical models for the forces and moments are required.

Flight systems with higher degrees of freedom and with aerodynamics that are nonlinear are beginning to be attacked from the standpoint of bifurcation theory (e.g., [49]). Here again much work needs to be done.

5. CONCLUDING REMARKS. This paper along with its companion paper at this conference, Mathematical Modeling of the Aerodynamic Characteristics in Flight Dynamics [1], is an attempt to provide a consistent formulation and theoretical method for studying nonlinear problems in flight dynamics. A description of a flight-dynamic system was presented in terms of its two major components, namely, the aerodynamic and inertial systems, and the coupling between them. Two important points follow from this description. First, because the aerodynamic system is governed by a set of nonlinear partial differential equations, the aerodynamic system represents a major source of nonlinearities in the flight-dynamic system. Second, the nonlinear aerodynamic forces and moments, which are the coupling from the aerodynamic system to the inertial system, in principle depend on the entire flight history and hence appear as functionals in the inertial system.

The aerodynamic system was examined in considerable detail and a framework to facilitate its study was proposed. The framework is composed of an observational and a mathematical component. A study of observations of fluid flows led to four important elements for the observational component. First, the flow patterns, although in many cases very complex, have definite structure (e.g., three-dimensional vortical structures). Second, these structures undergo systematic changes with variations in

parameters such as angle of attack or Reynolds number. Third, under some conditions these changes lead to chaos (e.g., turbulence). Although in reality a property of structure, because of its special importance in aerodynamics and its apparent incomprehensibility, chaos is treated as a separate element. Fourth, the structures have definite spatial or temporal scales.

The mathematical component that was proposed to deal with the four elements of the observational component emphasizes topological concepts that have considerable descriptive power, as well as the necessary depth to handle the essential nonlinearity of the problem. The mathematical presentation was intended to be descriptive, rather than rigorous, to highlight potential directions for future research. Structures of fluid flows were described by means of the topology of isolated critical points. Changes in the structures were examined in the light of bifurcation theory at two levels: one related to the classic study of stability of fluid-dynamic systems and the other to the structural stability of time-invariant structures. Chaos was examined in the light of recent studies of nonlinear dynamical systems. The idea here was to relate the occurrence of turbulence in fluid-dynamic systems to the chaotic behavior of deterministic dynamical systems that has been characterized by the existence of strange attractors having fractal dimensionality. The scales of structures were considered in the light of some ideas from group theory, beginning with classic dimensional analysis and touching on recent work in renormalized group theory.

Finally, a brief study was presented of some of the forms of flight-dynamic behavior that can result from the particular nonlinear aerodynamic

properties that were highlighted. The aerodynamic contributions to the inertial equations of motion had to be mathematically modeled in accordance with ideas summarized in the above-mentioned companion paper to this one. Three points can be made concerning this brief study of flight-dynamic behavior. First, in even a simple system having only one or two degrees of freedom, increasing complexity of the aerodynamic contribution causes flight-dynamic behavior to range from that corresponding to the presence of a fixed-point attractor to the chaotic motion corresponding to the presence of a strange attractor. Second, the mathematical ideas that have proved useful in describing fluid flows are found similarly useful in describing flight-dynamic behavior. Third, even a relatively simple mathematical model of the aerodynamic contribution to the inertial equations of motion can lead to flight-dynamic behavior that is sufficiently complex to exceed the range of validity of the aerodynamic model that was assumed. This emphasizes the importance of understanding the strong interdependence that exists between the level of our knowledge of nonlinear aerodynamic phenomena, our means of mathematically modeling them, and the range of nonlinear flight-dynamic behavior that results.

REFERENCES

1. M. Tobak, G. T. Chapman, and L. B. Schiff, Mathematical Modeling of the Aerodynamic Characteristics in Flight Dynamics, Berkeley-Ames Conference on Nonlinear Problems in Control and Fluid Dynamics, Berkeley, Calif., May-June 1983.

2. M. Fiechter, Ober Wirebelsystome an Schlanken Rotationskörpern und Ihren Einfluss auf dis Aerodynamischen Buiwerte, Deutsch-Franzosisches Forschungsinstitut Saint-Louis Rapport 10/66, Dec. 1966.

3. G. T. Chapman, M. Tobak, and L. B. Schiff, The Role of Computational Fluid Dynamics in Flight Mechanics, AIAA Paper 83-2075, Gatlinberg, Tenn., Aug. 1983.

4. M. V. Morkovin, Flow Around Circular Cylinders — A Kaleidoscope of Challenging Fluid Phenomena, Symposium on Fully Separated Flows, American Society of Mechanical Engineers, 1964.

5. R. Legendre, Séparation de l'Écoulement Laminaire Tridimensionel, Rech Aéro., Vol. 54 (1956), pp. 3-8.

6. R. Legendre, Lignes de Courant d'un Écoulement Continu, Rech Aérosp., Vol. 105 (1965), pp. 3-9.

7. J. C. R. Hunt, C. J. Abell, J. A. Peterka, and H. Woo, Kinematical Studies of the Flows Around Free or Surface-Mounted Obstacles; Applying Topology to Flow Visualization, J. Fluid Mech., Vol. 86, Pt. 1, (1978), pp. 179-200.

8. M. Tobak and D. J. Peake, Topology of Three-Dimensional Separated Flows, Annu. Rev. Fluid Mech., Vol. 14 (1982), pp. 61-85.

9. H. G. Hornung, The Vortex Skeleton for 3-D Steady Flows, AGARD CP 342 Aerodynamics of Vortical Types of Flow in Three-Dimensions, pp. 2-1 to 2-12, 1983.

10. D. D. Joseph, Stability of Fluid Motions I, Berlin Springer, 1976.

11. E. N. Lorenz, Deterministic Nonperiodic Flow, J. Atmos. Sci., Vol. 20 (1963), pp. 130-141.

12. D. Ruelle and F. Takens, On the Nature of Turbulence, Commun. Math. Physics, Vol. 20 (1971), pp. 167-192.

13. B. B. Mandelbrot, The Fractal Geometry of Nature, W. H. Freeman, San Francisco, 1982.

14. P. W. Bridgeman, Dimensional Analysis, Yale University Press, 1922.

15. H. Schlichting, Boundary Layer Theory, McGraw-Hill, New York, 1955.

16. M. Van Dyke, An Album of Fluid Motion, The Parabolic Press, 1982.

17. J. H. Jones and J. E. O'Hare, Flow Visualization of a Yawed Tangent-Ogive Cylinder at Mach Number 2, AEDC-TR-73-45, 1973.

18. D. J. Peake and M. Tobak, On Issues Concerning Flow Separation and Vortical Flows in Three Dimensions, AGARD CP-342, Aerodynamics of Vortical Types of Flow in Three-Dimensions, pp. 1-1 to 1-31, 1983.

19. R. Thom, Stabilité Structurelles et Morphogenèse, New York, Benjamin (Transl. Structural Stability and Morphogenesis, Reading Benjamin, 1975).

20. D. H. Sattinger, Bifurcation and Symmetry Breaking in Applied Mathematics, Bull. (New Series) Amer. Math. Soc., Vol. 3 (1980), pp. 779-819.

21. M. Golubitsky and D. Schaeffer, Imperfect Bifurcation in the Presence of Symmetry, Commun. Math. Phys., Vol. 67 (1979), pp. 205-232.

22. J. Guckenheimer and P. Holmes, Nonlinear Oscillations, Dynamical Systems, and Bifurcations of Vector Fields, Springer-Verlag, New York, 1983.

23. T. Poston and I. Stewart, Catastrophe Theory and Applications, Pitman, 1978.

24. A. Skow and G. E. Erickson, Modern Aircraft Design for High Angle of Attack Maneuvering, AGARD LS-121, No. 4, Dec. 1982.

25. M. G. Hall, Vortex Breakdown, Annu. Rev. Fluid Mech., Vol. 4, (1972), pp. 195-218.

26. J. H. Faler and S. Leibovich, Disrupted States of Vortex Flow and Vortex Breakdown, The Phys. Fluids, Vol. 20, No. 9 (1977), pp. 1385-1400.

27. M. V. Lowson, Some Experiments with Vortex Breakdown, J. Royal Aero. Soc., Vol. 68 (1964), pp. 343-346.

28. G. N. Malcolm and M. H. Clarkson, Wind Tunnel Testing with a Rotary-Balance Apparatus to Simulate Aircraft Spin Motions, pp. 143-146, Proceedings AIAA 9th Aerodynamics Testing Conf., Arlington, Tex., June 1976.

29. C. S. James, Observations of Turbulent-Burst Geometry and Growth in Supersonic Flow, NACA TN-4235, 1958.

30. L. Landau, On the Problem of Turbulence, C. R. Acad. Sci. USSR, Vol. 44 (1944), p. 311.

31. J. P. Eckmann, Roads to Turbulence in Dissipative Dynamical Systems, Rev. Mod. Phys., Vol. 53, No. 4, Pt. 1 (Oct. 1981), pp. 643-654.

32. C. Sparrow, The Lorenz Equations: Bifurcations, Chaos, and Strange Attractors, Springer-Verlag, New York, 1982.

33. P. Moin and J. Kim, Numerical Investigation of Turbulent Channel Flow, J. Fluid Mech., Vol. 118 (1982), pp. 341-377.

34. O. E. Lanford, III, The Strange Attractor Theory of Turbulence, Annu. Rev. Fluid Mech., Vol. 14 (1982), pp. 347-364.

35. E. Ott, Strange Attractors and Chaotic Motions of Dynamical Systems, Rev. Modern Phys., Vol. 53, No. 4, Pt. 1 (1981), pp. 655-671.

36. G. K. Batchelor and A. A. Townsend, The Nature of Turbulent Motion at High Wave Number, Proc. R. Soc. London, Series A, Vol. 199 (1949), pp. 238-255.

37. A. J. Chorin, The Evolution of a Turbulent Vortex, Commun. Math. Phys., Vol. 83 (1982), pp. 517-535.

38. J. J. Cornish, III, Vortex Flows, presented at the Eighth Quick-Goethert Lecture Series at the University of Tennessee Space Institute, Tullahoma, Tenn., Oct. 1982.

39. M. Van Dyke, Perturbation Methods in Fluid Mechanics, Academic Press, New York and London, 1964.

40. L. Prandtl, Über die Ausgebildete Turbulenz, Zamm, Vol. 5 (1925).

41. S. J. Kline et al., Proceedings of the AFOSR-IFP-Stanford Conference on Computations of Turbulent Boundary Layers, Vols. I and II, Stanford University, Stanford, Calif., 1968.

42. J. S. Shang and W. L. Hankey, Jr., Supersonic Turbulent Flows Utilizing the Navier-Stokes Equations, AGARD-CPP-168, May 1975, pp. 23-31.

43. K. G. Wilson and J. Kogut, The Renormalization Group and the ε Expansion, Physics Report C, Vol. 12, No. 2 (1974), pp. 75-200.

44. M. J. Feigenbaum, L. P. Kadanoff, and S. J. Shenker, Quasi-Periodicity in Dissipative Systems: A Renormalized Group Analysis, Physica 5D (1982), pp. 370-386.

45. E. D. Siggia, Numerical Studies of Small-Scale Intermittency in Three-Dimensional Turbulence, J. Fluid Mech., Vol. 107 (1981), pp. 375-406.

46. A. L. Robinson, Physicists Try to Find Order in Chaos, Science, Vol. 218 (1982), pp. 554-556.

47. K. W. McAlister and L. W. Carr, Water-Tunnel Experiments on an Oscillating Airfoil at Re = 21,000, NASA TM-78446, Mar. 1978.

48. K. W. McAlister, L. W. Carr, and W. J. McCroskey, Dynamic Stall Experiments on the NACA 0012 Airfoil, NASA TP-1100, Jan. 1978.

49. J. V. Carroll and R. K. Mehra, Bifurcation Analysis on Nonlinear Aircraft Dynamics, J. Guidance, Control, and Dynamics, Vol. 5, No. 5 (1982) pp. 529-536.

50. P. Guicheteau, Application de la Theorie des Bifurcations à l'Étude des Pertes de Controle sur Avion de Combat, Paper No. 17, AGARD CP 319, Combat Aircraft Maneuverability, 1981.

51. W. H. Hui and M. Tobak, Bifurcation Analysis of Aircraft Pitching Motions Near the Stability Boundary, Berkeley-Ames Conference on Nonlinear Problems in Control and Fluid Mechanics, Berkeley, Calif., 1983.

52. P. Holmes and R. Rand, Phase Portraits and Bifurcations of the Nonlinear Oscillator: $\ddot{x} + (\alpha + \gamma x^2)\dot{x} + \beta x + \delta x^3 = 0$, J. Nonlinear Mech., Vol. 15 (1980), pp. 449-458.

53. M. Diener and T. Poston, On the Perfect Delay Convention or the Revolt of the Slaved Variables, in Chaos and Order in Nature, edited by H. Haken, Berlin Springer, 1981.

FIGURE CAPTIONS

Fig. 1. Elements of flight-dynamic systems.

Fig. 2. Block diagram of a rigid-body flight-dynamic system.

Fig. 3. Vortex flow on a slender body in a water tunnel; U = 4 cm/sec, Re = 400.

Fig. 4. Nonlinear aerodynamics; normal-force coefficient of a slender body.

Fig. 5. Critical points.

Fig. 6. Vapor screen of vortex flow on a slender body in a wind tunnel; $M = 2.0$, $\alpha = 21.2°$.

Fig. 7. Crossflow topologies for slender body of revolution at increasing angles of attack.

Fig. 8. Surface streamlines on a wing at transonic speeds; $Re = 6.8 \times 10^6$, $\alpha = 5°$.

Fig. 9. Bifurcation diagrams; some examples.

Fig. 10. Crossflow topologies and bifurcations for a slender body of revolution with increasing angle of attack.

Fig. 11. Vortex breakdown on a swept wing in a water tunnel.

Fig. 12. Aerodynamic hysteresis; asymmetric vortex breakdown on a slender delta wing.

Fig. 13. Aerodynamic hysteresis; flow separation on a spinning body with a square cross section: nose side force at $\alpha = 90°$.

Fig. 14. Turbulent boundary layer flow on a hollow circular cylinder in free flight: $M = 3.1$, $Re = 20 \times 10^6$.

Fig. 15. A strange attractor: Lorenz attractor.

Fig. 16. Perturbation velocity contours from a turbulent channel flow calculation.

Fig. 17. Fractals — some examples.

Fig. 18. Resolution of critical points.

Fig. 19. Two scales; spiral nodes.

Fig. 20. Aerodynamics of an oscillating airfoil: dynamic stall.

Fig. 21. Summary of aerodynamic forces.

Fig. 22. Flight-dynamic characteristics: a single-degree-of-freedom system.

Fig. 23. Flight dynamics: example of phase plane characteristics.

Fig. 24. Flight-dynamic characteristics with aerodynamic hysteresis: two-degrees-of-freedom system.

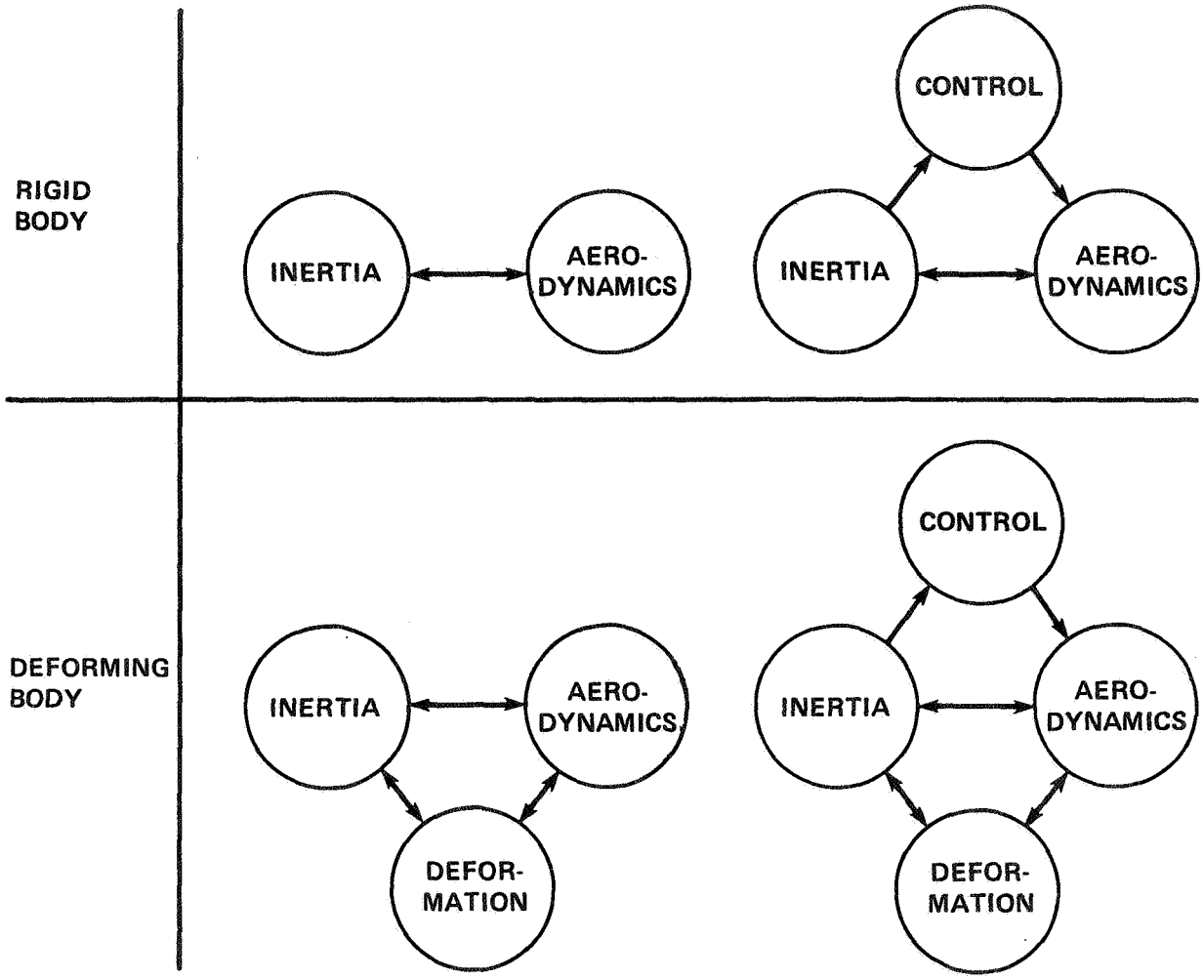
RIGID BODY
INERTIA
AERO-DYNAMICS
CONTROL
INERTIA
AERO-DYNAMICS
DEFORMING BODY
INERTIA
AERO-DYNAMICS
DEFOR-MATION
CONTROL
INERTIA
AERO-DYNAMICS
DEFOR-MATION

Fig. 1

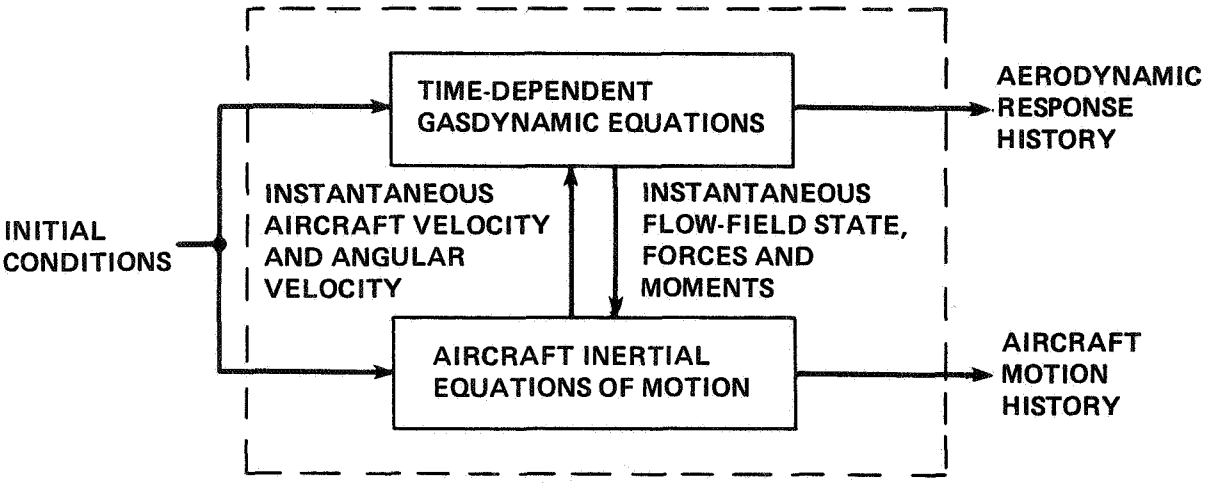
TIME-DEPENDENT
GASDYNAMIC EQUATIONS
AERODYNAMIC
RESPONSE
HISTORY
INITIAL
CONDITIONS
INSTANTANEOUS
AIRCRAFT VELOCITY
AND ANGULAR
VELOCITY
INSTANTANEOUS
FLOW-FIELD STATE,
FORCES AND
MOMENTS
AIRCRAFT INERTIAL
EQUATIONS OF MOTION
AIRCRAFT
MOTION
HISTORY

Fig. 2

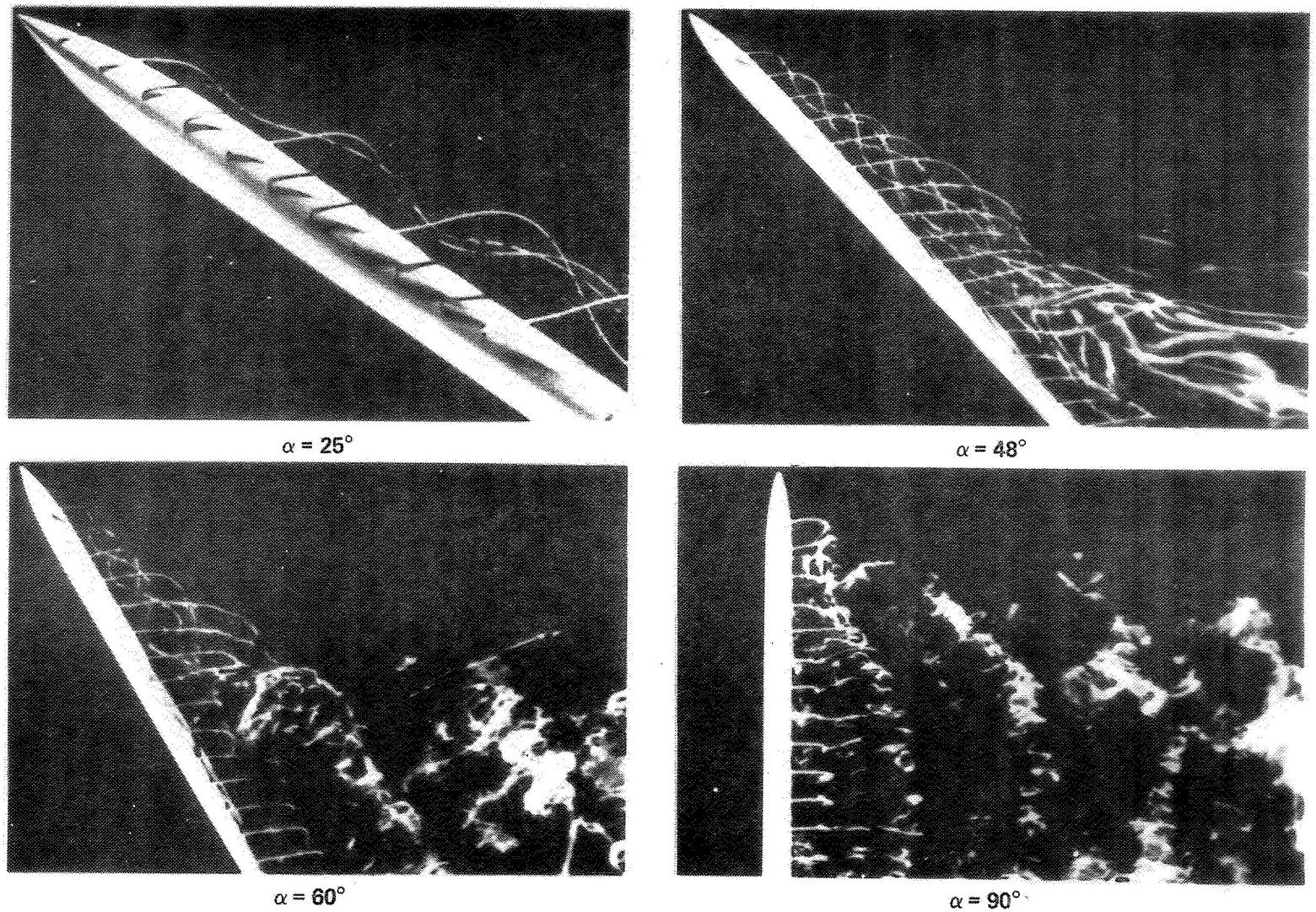

Fig. 3

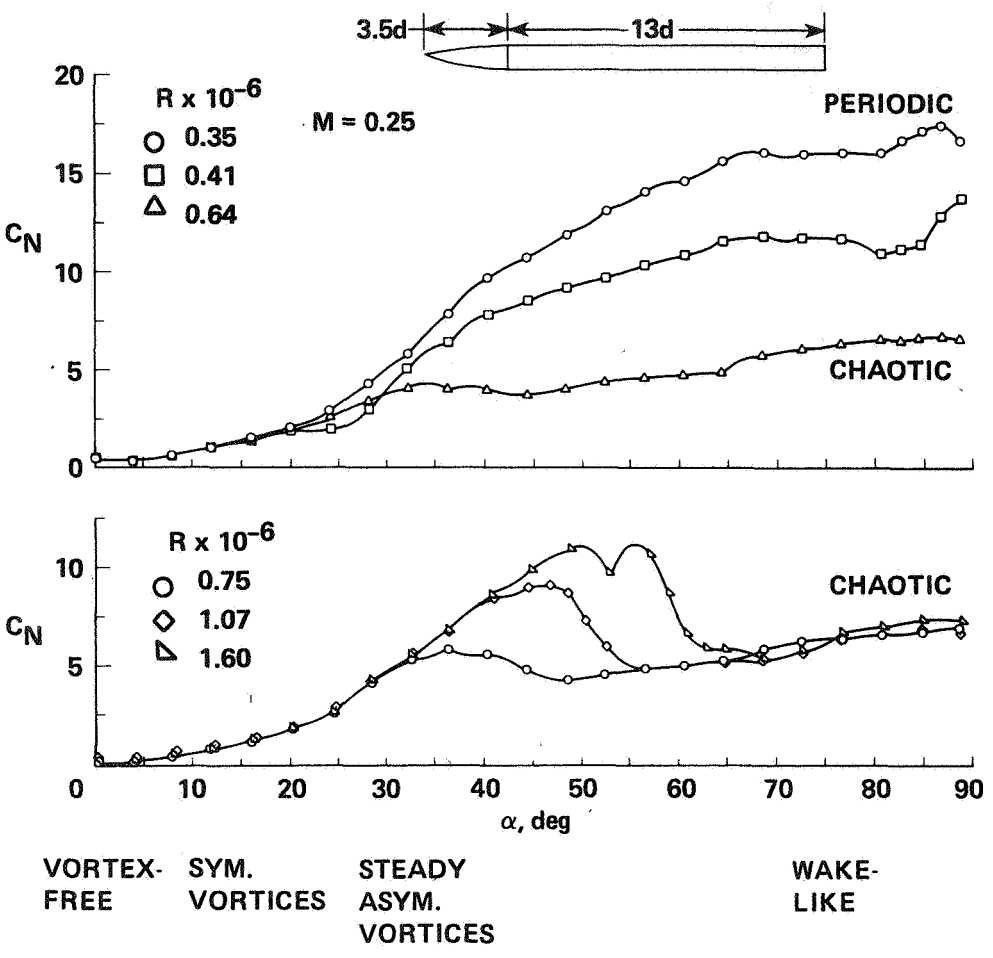
3.5d
13d
20
15
10
5
0
C_N
R x 10^{-6}
0.35
0.41
0.64
M = 0.25
PERIODIC
CHAOTIC
R x 10^{-6}
0.75
1.07
1.60
CHAOTIC
0
10
20
30
40
50
60
70
80
90
α, deg
VORTEX-FREE
SYM. VORTICES
STEADY ASYM. VORTICES
WAKE-LIKE

Fig. 4

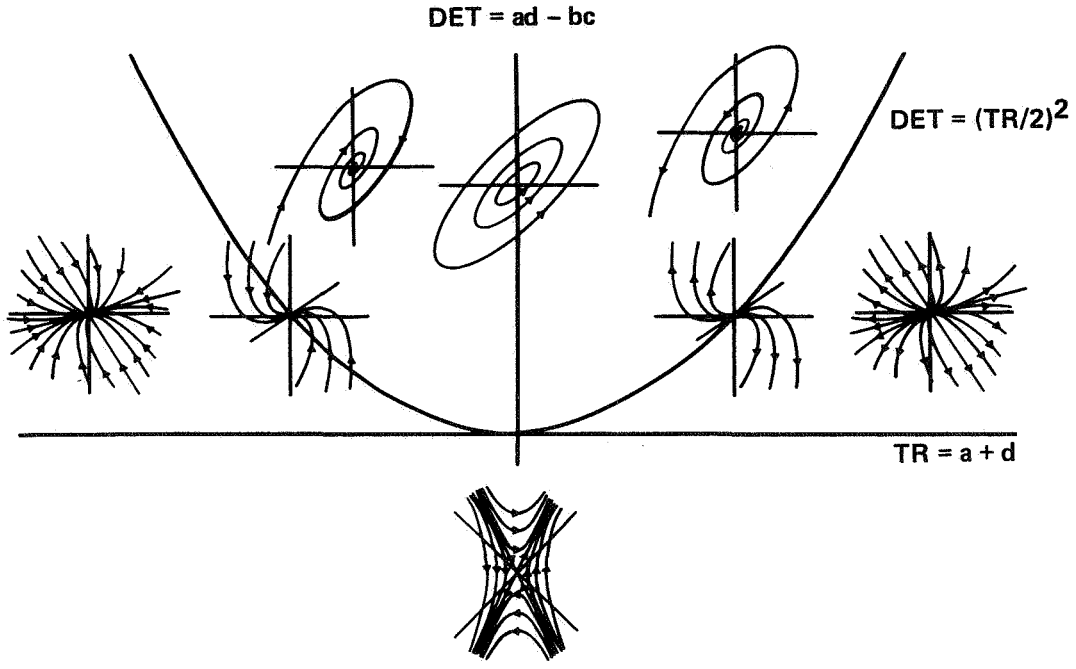

Fig. 5

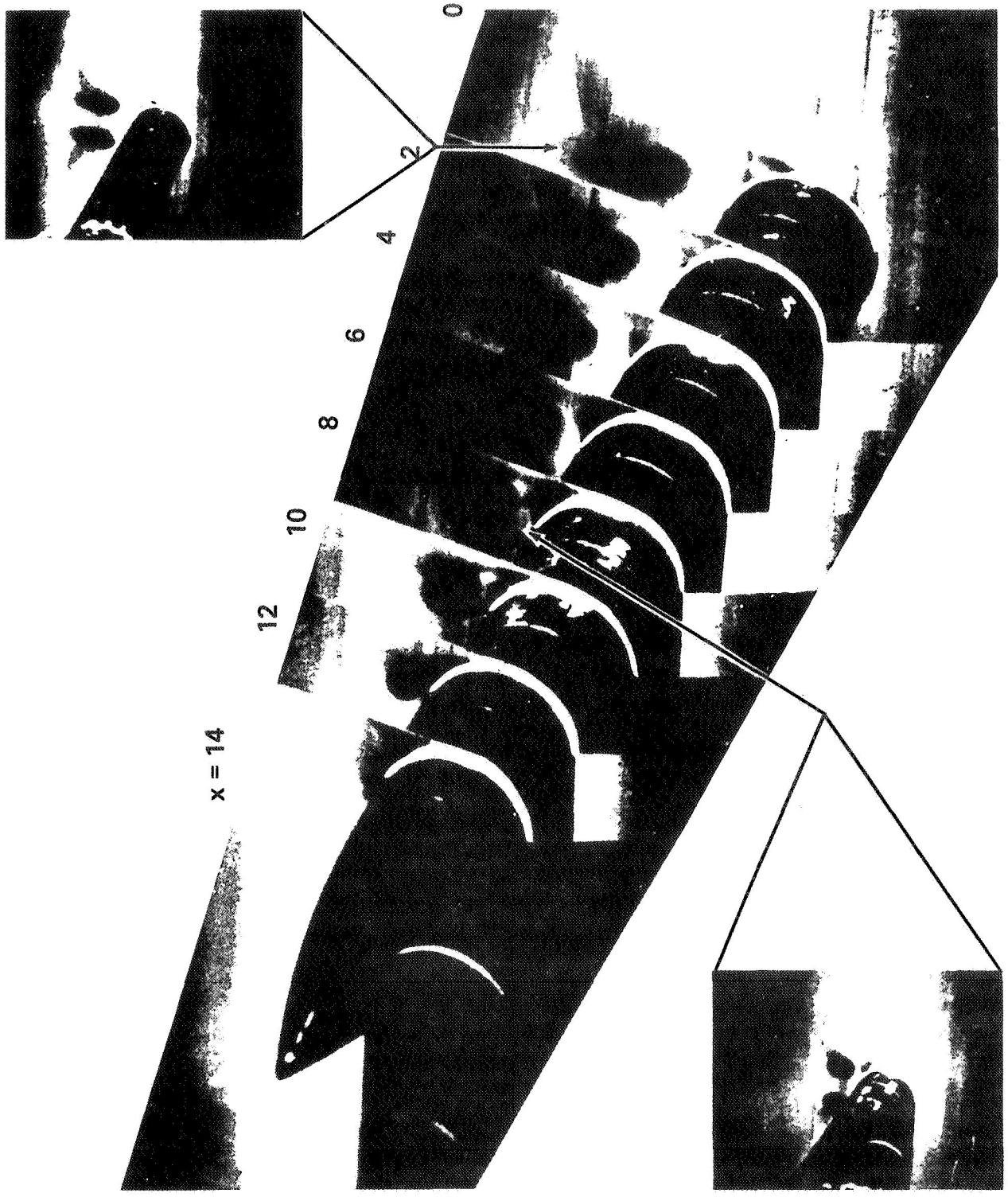

Fig. 6

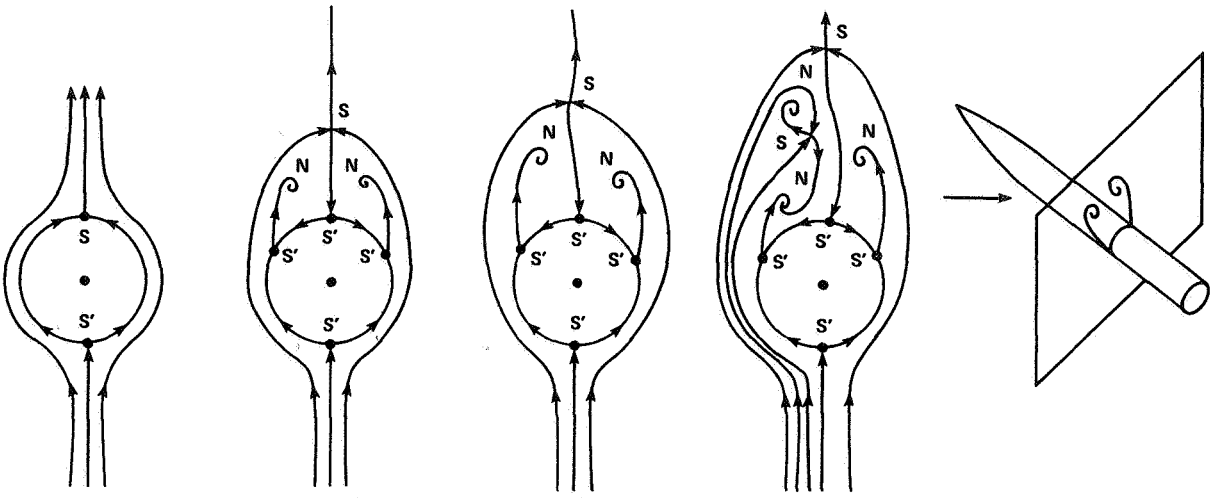

VORTEX FREE	SYMMETRIC VORTEX	ASYMMETRIC VORTEX	ASYMMETRIC VORTEX
N = 0	2	2	3
N' = 0	0	0	0
S = 0	1	1	2
S' = 2	4	4	4
Σ = -1	-1	-1	-1

INCREASING ANGLE OF ATTACK ⟶

Fig. 7

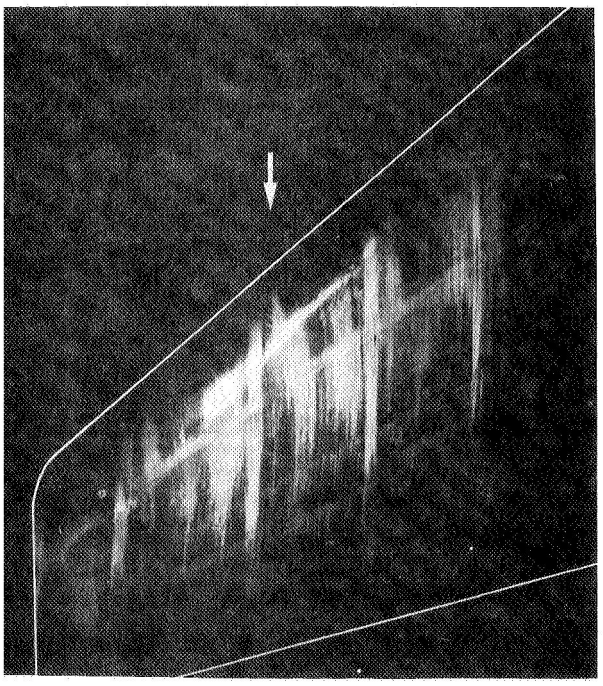

ATTACHED
M = 0.82

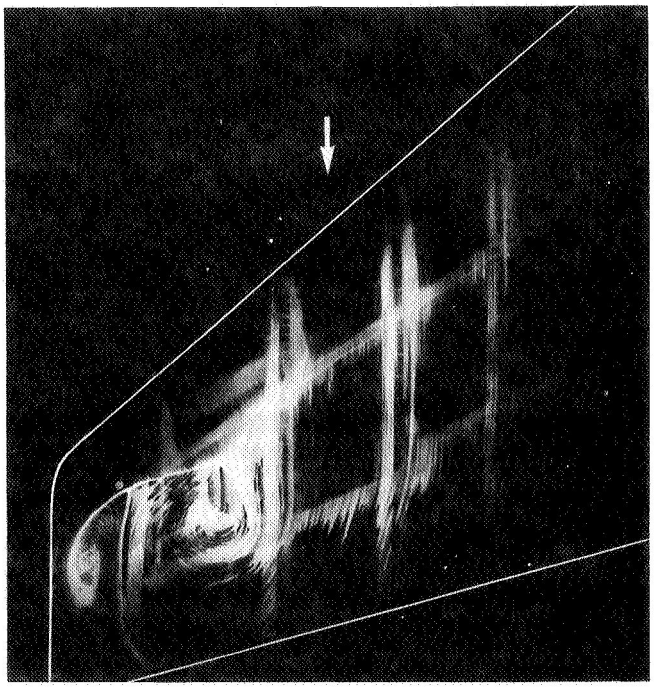

SEPARATED
M = 0.90

Fig. 8

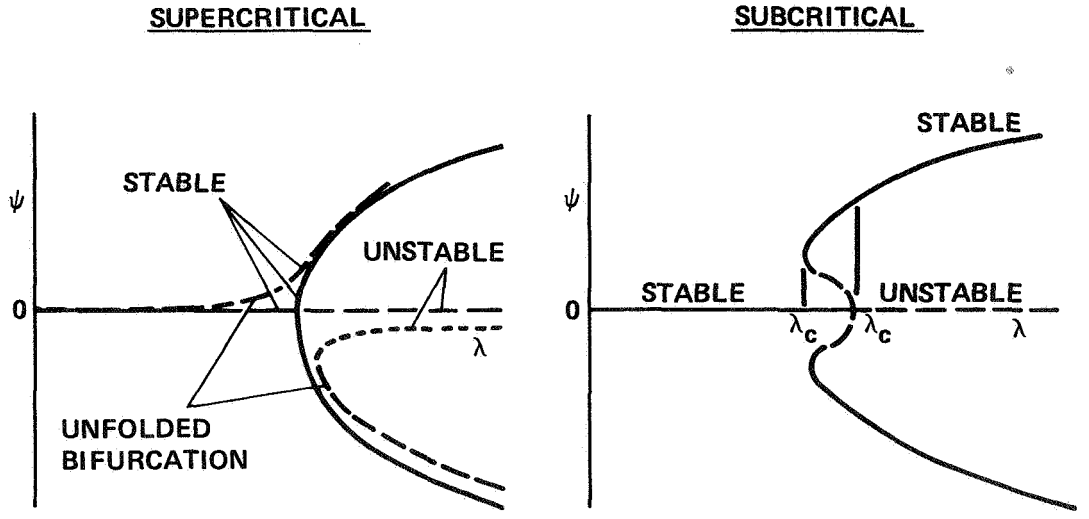
SUPERCRITICAL
SUBCRITICAL
STABLE
UNSTABLE
UNFOLDED
BIFURCATION
ψ
0
λ
STABLE
STABLE
UNSTABLE
λ_c
λ_c

Fig. 9

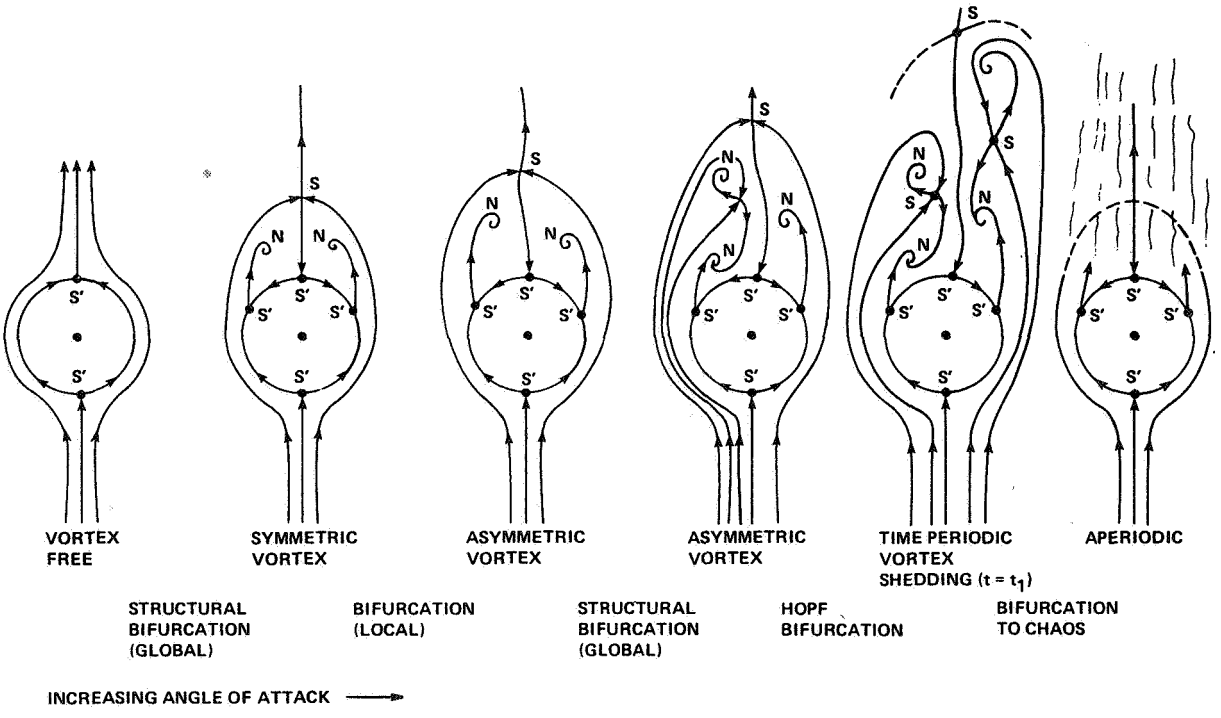
VORTEX FREE
SYMMETRIC VORTEX
ASYMMETRIC VORTEX
ASYMMETRIC VORTEX
TIME PERIODIC VORTEX SHEDDING (t = t1)
APERIODIC
STRUCTURAL BIFURCATION (GLOBAL)
BIFURCATION (LOCAL)
STRUCTURAL BIFURCATION (GLOBAL)
HOPF BIFURCATION
BIFURCATION TO CHAOS
INCREASING ANGLE OF ATTACK

Fig. 10

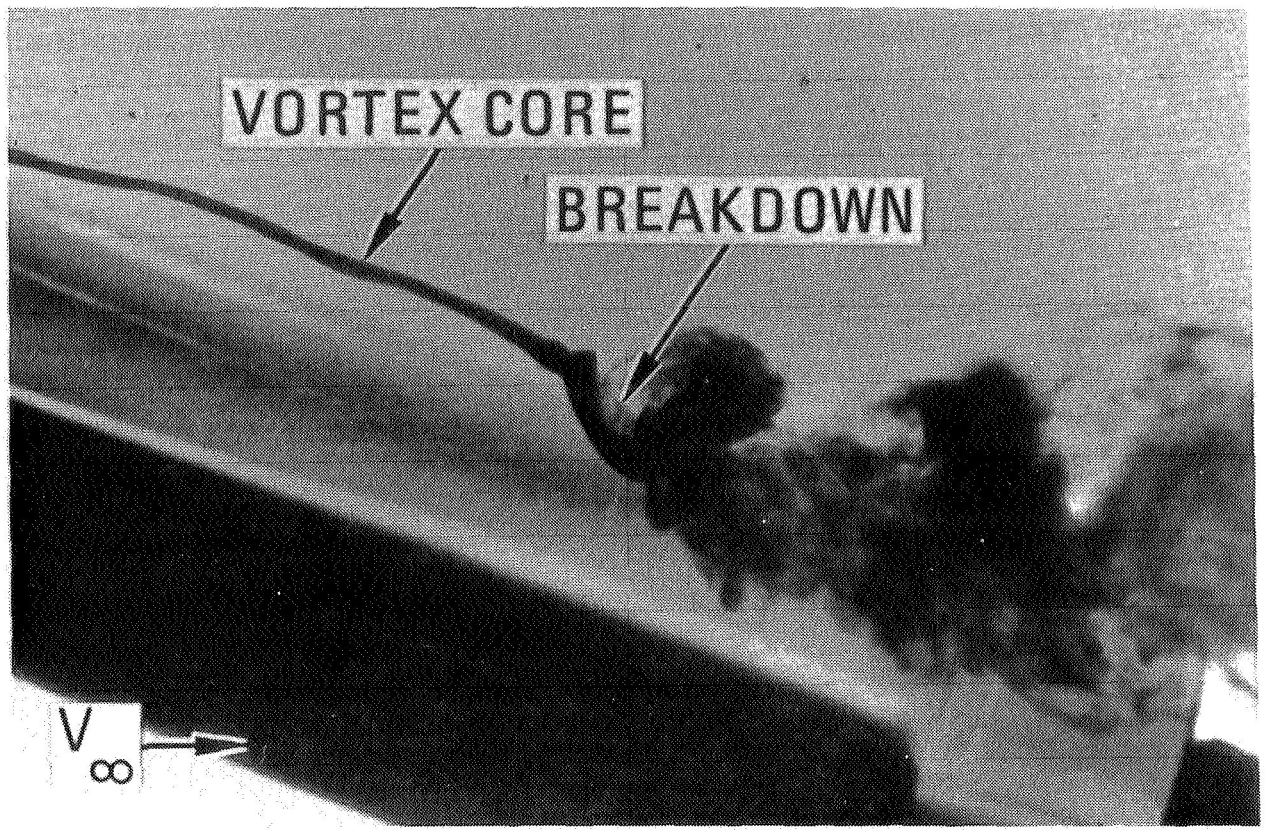

Fig. 11

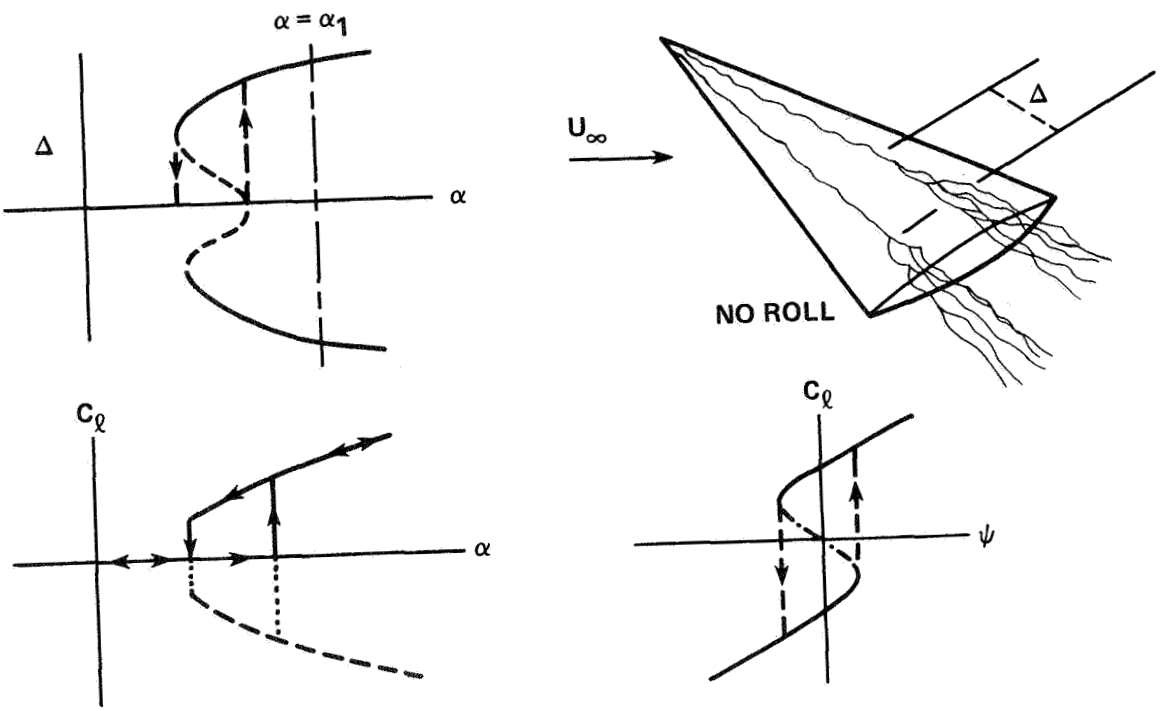

Fig. 12

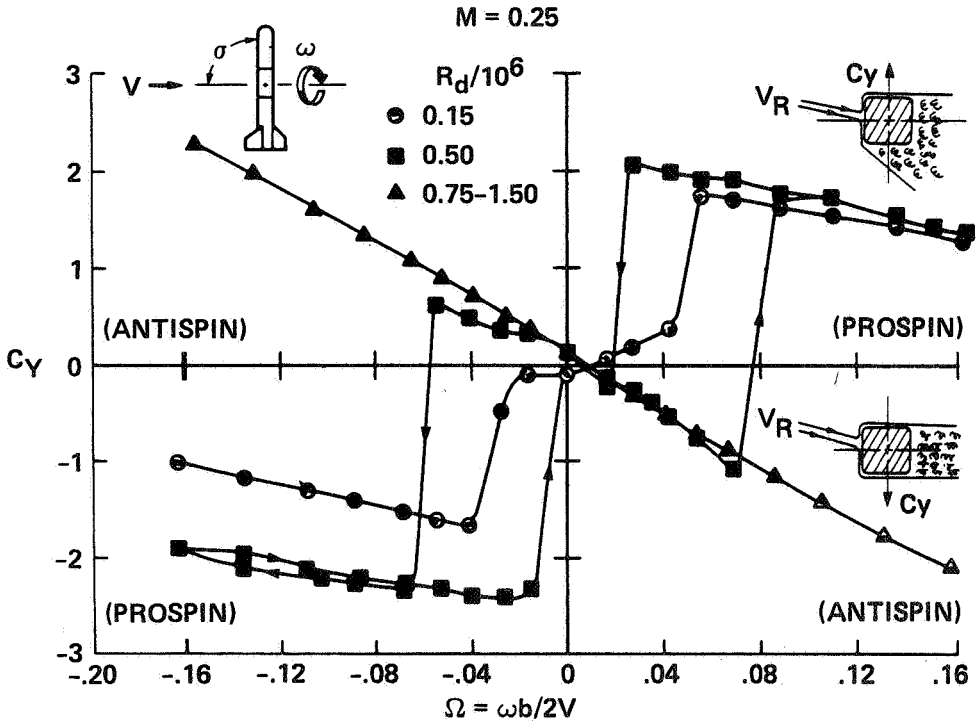
M = 0.25
V
σ
ω
$R_d/10^6$
0.15
0.50
0.75-1.50
Cy
V_R
(ANTISPIN)
(PROSPIN)
C_Y
V_R
Cy
(PROSPIN)
(ANTISPIN)
3
2
1
0
-1
-2
-3
-.20
-.16
-.12
-.08
-.04
0
.04
.08
.12
.16
$\Omega = \omega b/2V$

Fig. 13

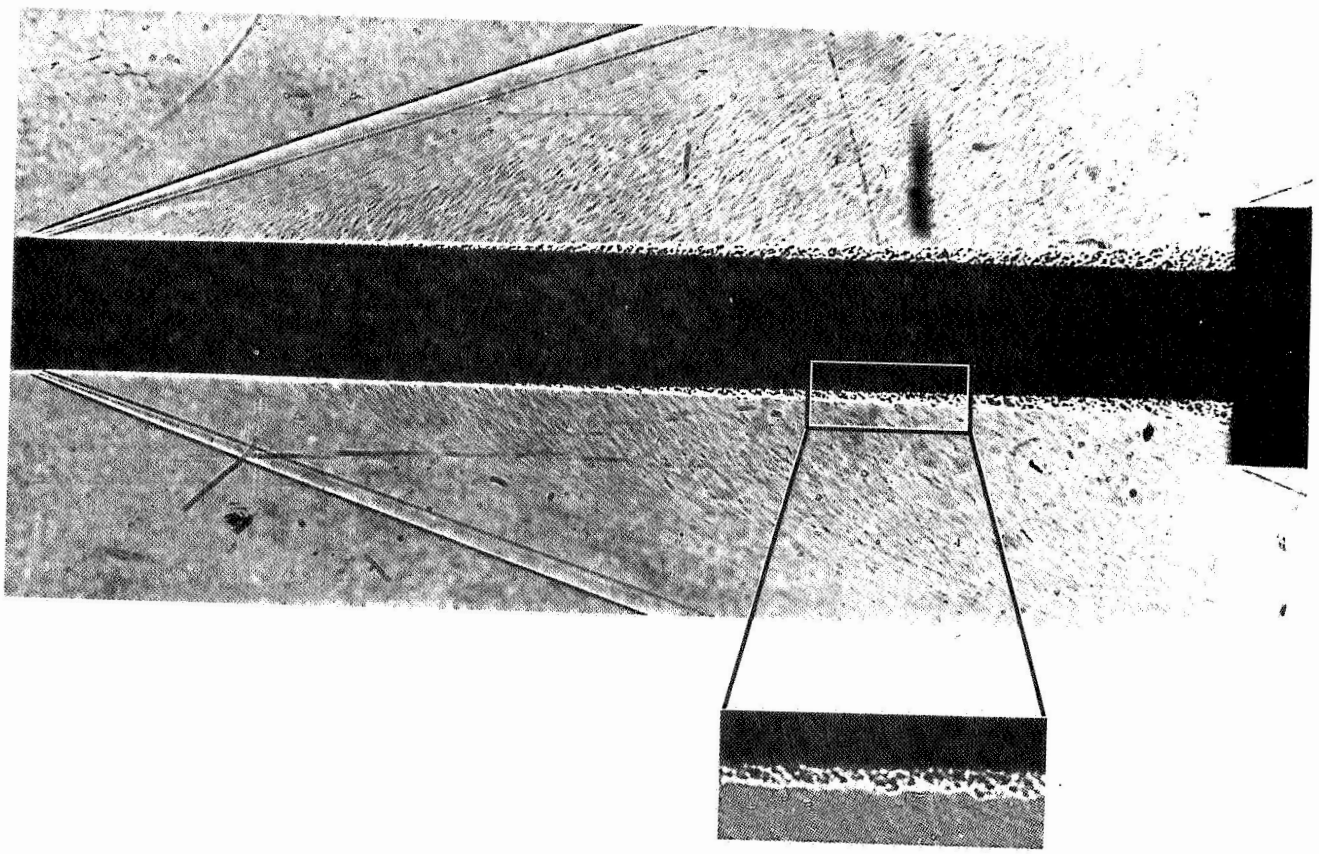

Fig. 14

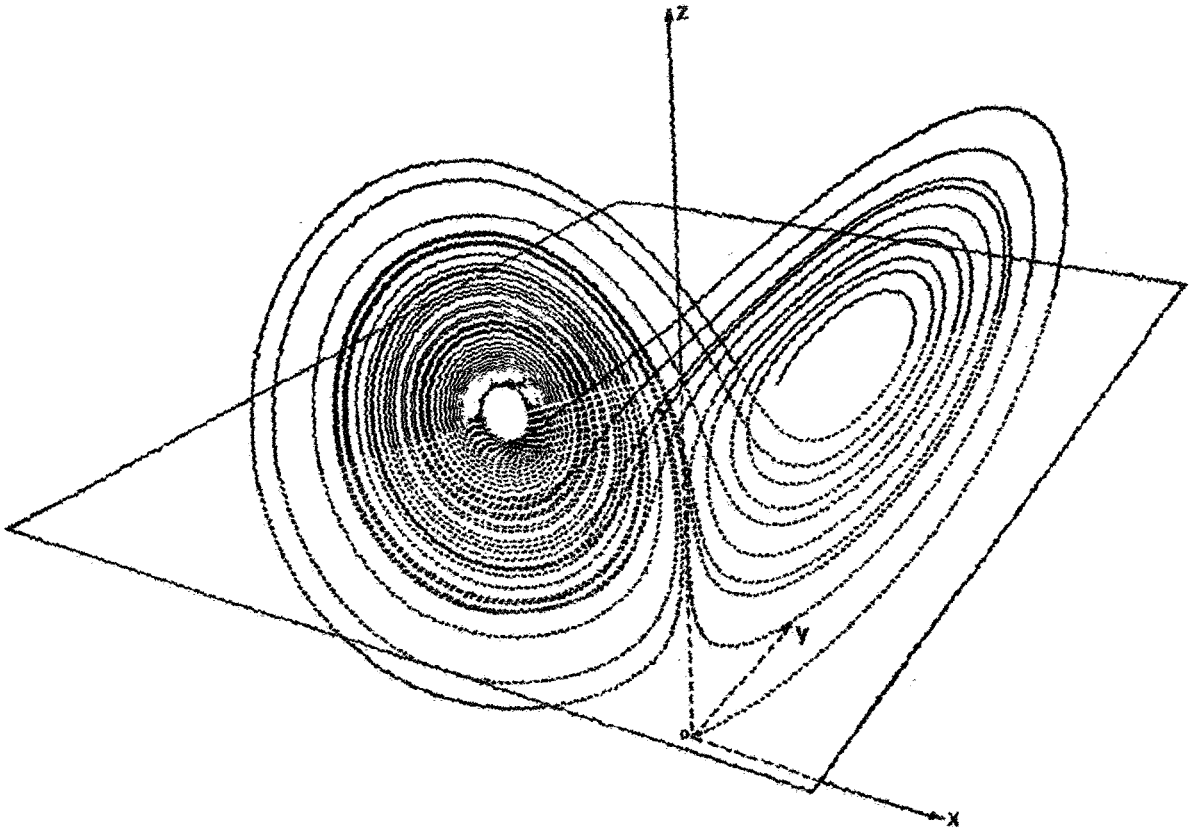

Fig. 15

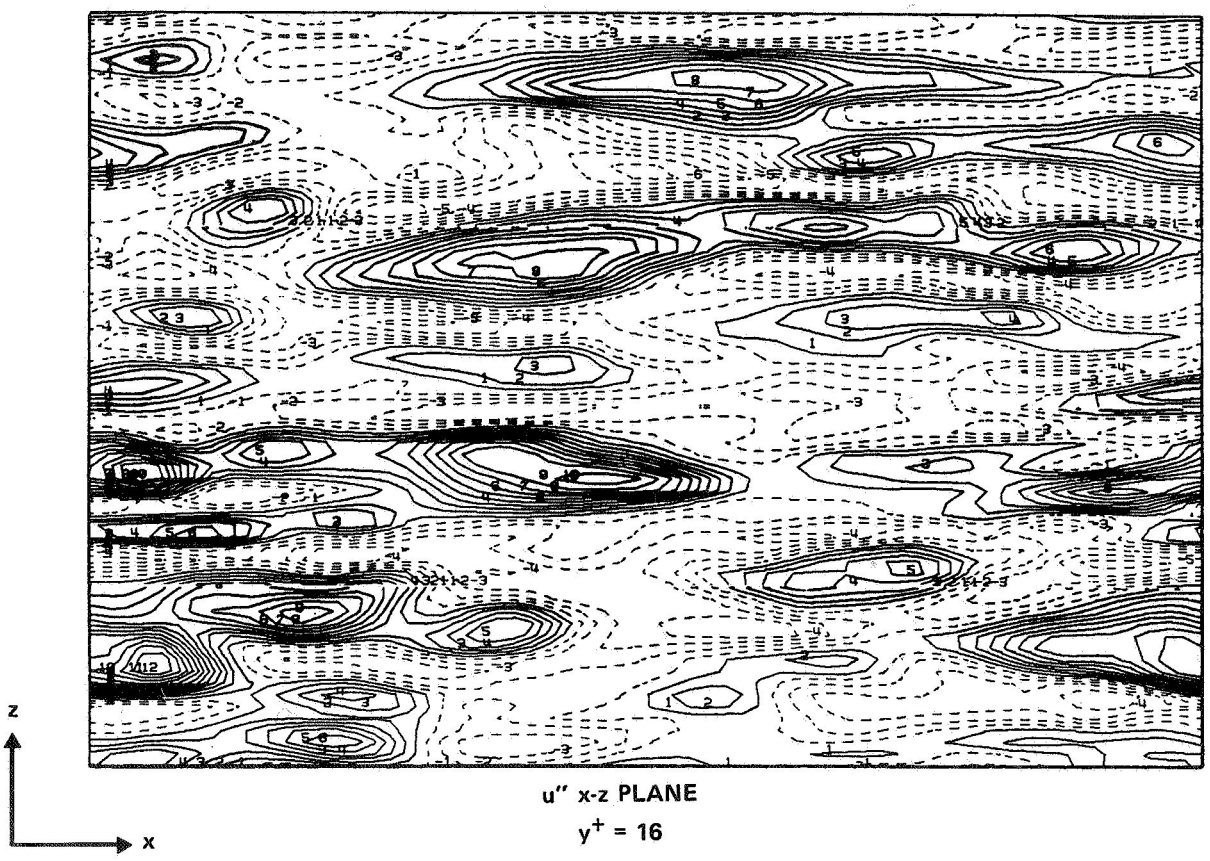

u'' x-z PLANE

$y^+ = 16$

Fig. 16

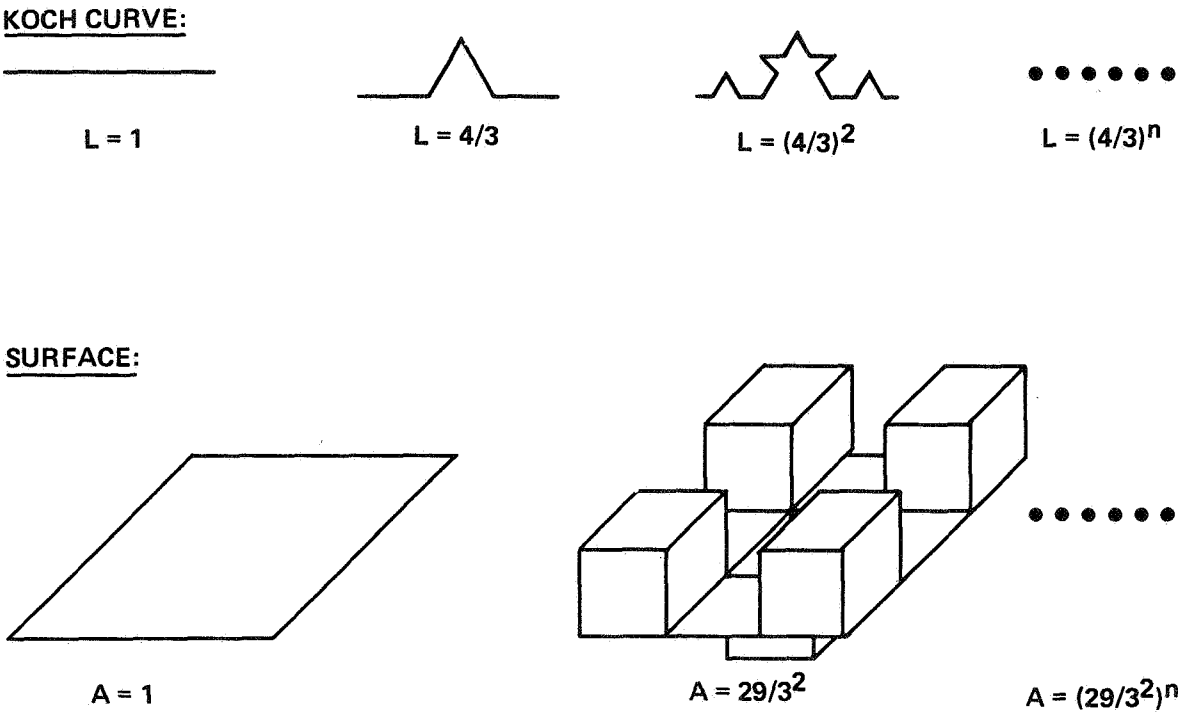

Fig. 17

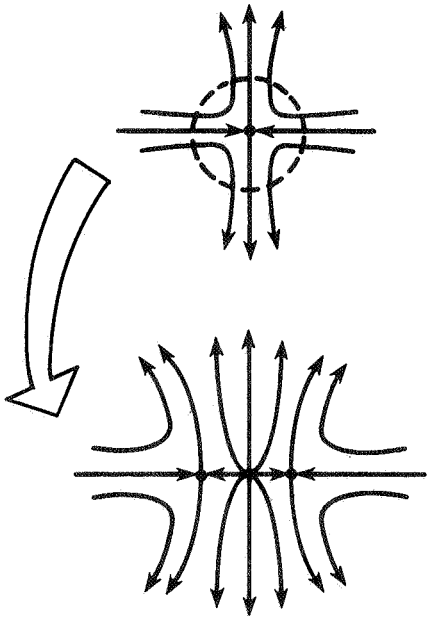

Fig. 18

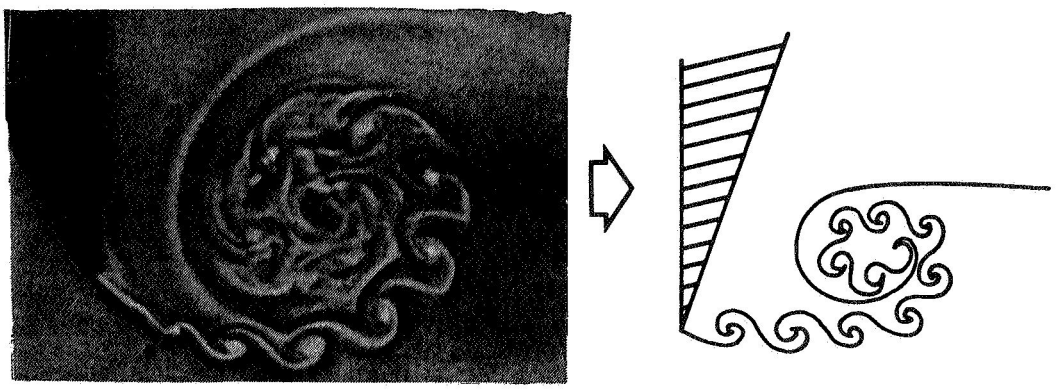

Fig. 19

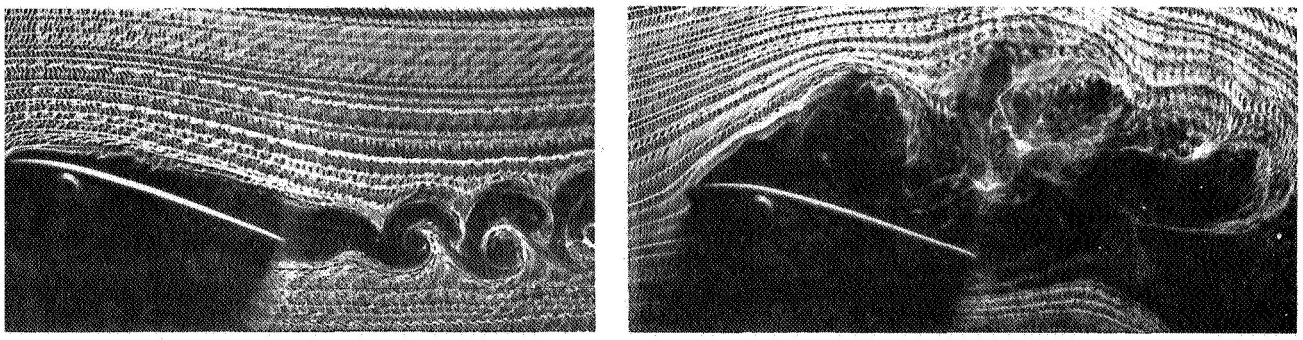

$\alpha = 15°, \dot{\alpha} > 0, k = 0.25$

$\alpha = 10° + 10° \sin \omega t$
(McALISTER AND CARR)

$\alpha = 15°, \dot{\alpha} < 0, k = 0.25$

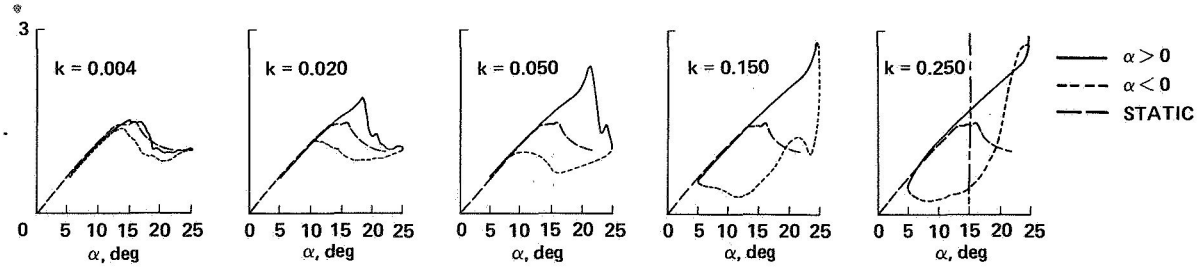

$\alpha = 15° + 10° \sin \omega t$
(McALISTER, CARR AND McCROSKEY)

Fig. 20

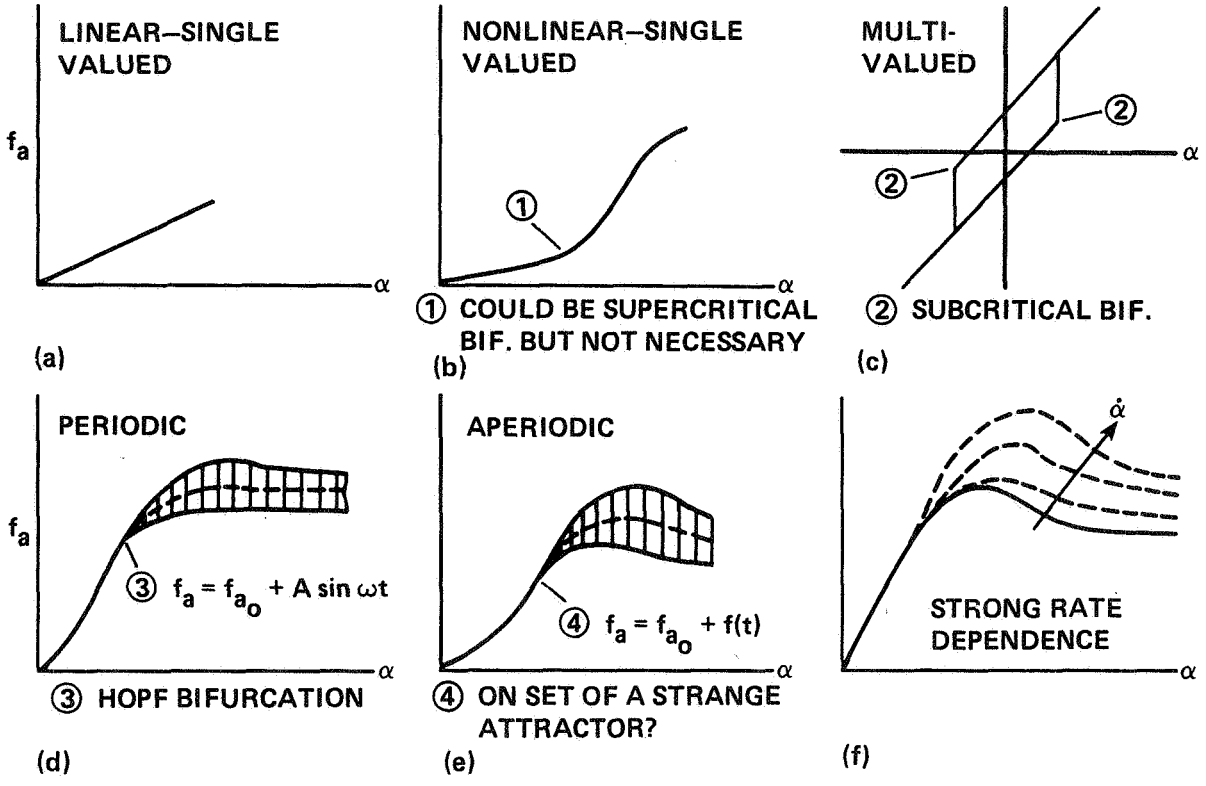
LINEAR–SINGLE VALUED
f_a
α
(a)
NONLINEAR–SINGLE VALUED
①
α
① COULD BE SUPERCRITICAL BIF. BUT NOT NECESSARY
(b)
MULTI-VALUED
②
②
α
② SUBCRITICAL BIF.
(c)
PERIODIC
f_a
③ $f_a = f_{a_o} + A \sin \omega t$
α
③ HOPF BIFURCATION
(d)
APERIODIC
④ $f_a = f_{a_o} + f(t)$
α
④ ON SET OF A STRANGE ATTRACTOR?
(e)
$\dot{\alpha}$
STRONG RATE DEPENDENCE
α
(f)

Fig. 21

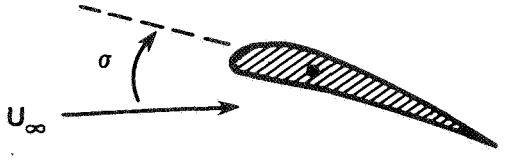

AERODYNAMICS	1-D FREEDOM 2ND ORDER EQ.	SOME CHARACTERISTICS
LINEAR $\sigma, \dot{\sigma}$	$\ddot{\sigma} + \underline{A\dot{\sigma} + B\sigma} = 0$	SINGLE CRITICAL POINT (CLASSICAL)
NONLINEAR σ LINEAR $\dot{\sigma}$	$\ddot{\sigma} + \underline{A(\sigma)\dot{\sigma} + B(\sigma)\sigma} = 0$ LIENARD EQ.	MULTIPLE CRITICAL POINTS LIMIT CYCLES SUPER-AND SUB-CRITICAL BIFURCATIONS
HYSTERESIS σ LINEAR $\dot{\sigma}$	$\ddot{\sigma} + \underline{A(\sigma, h)\dot{\sigma} + B(\sigma, h)\sigma} = 0$	MULTIPLE CRITICAL POINTS LIMIT CYCLES BOUNDED APERIODIC?
PERIODIC	$\ddot{\sigma} + \underline{[\ ?\ ]} = 0$	DYNAMIC STALL "LOCK IN"
BOUNDED APERIODIC	$\ddot{\sigma} + \underline{[\ ?\ ]} = 0$	BUFFETING

Fig. 22

$$\ddot{\sigma} + A(\sigma)\dot{\sigma} + B(\sigma)\sigma = 0$$

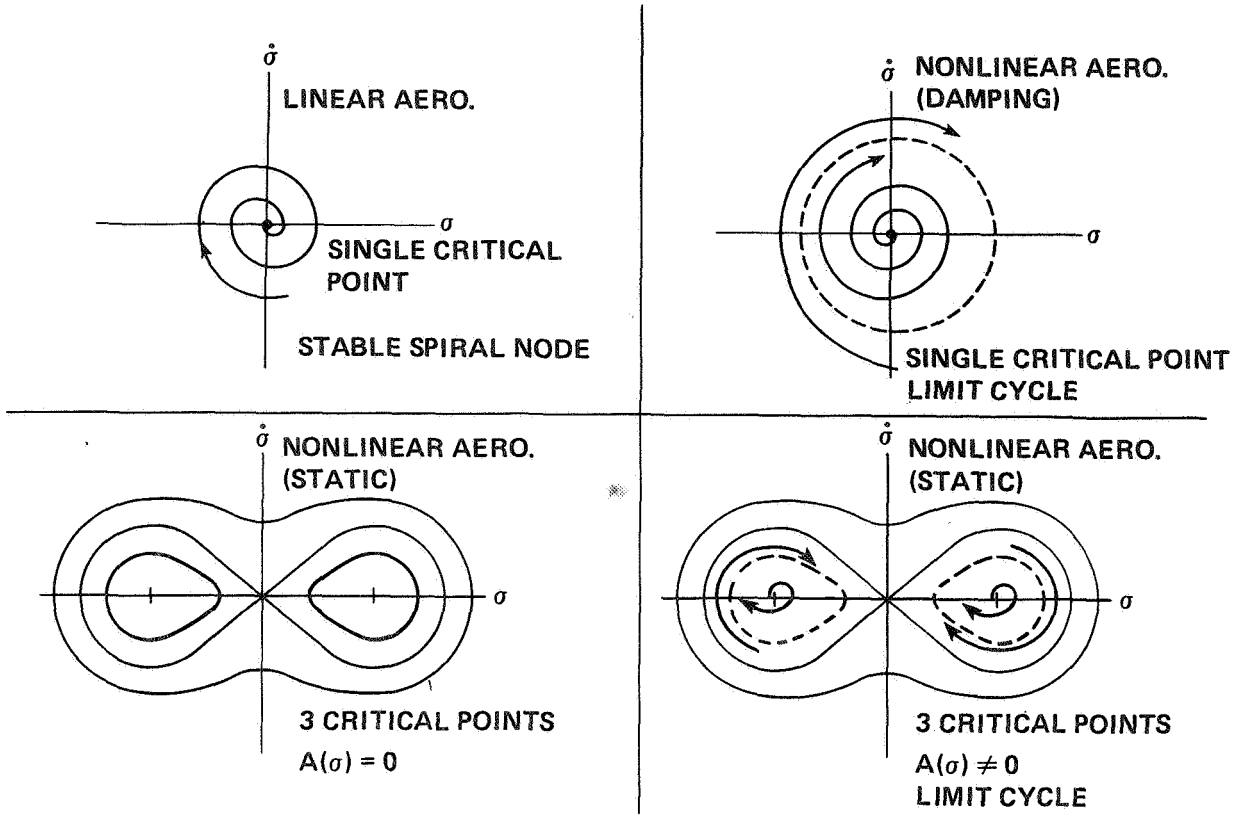

Fig. 23

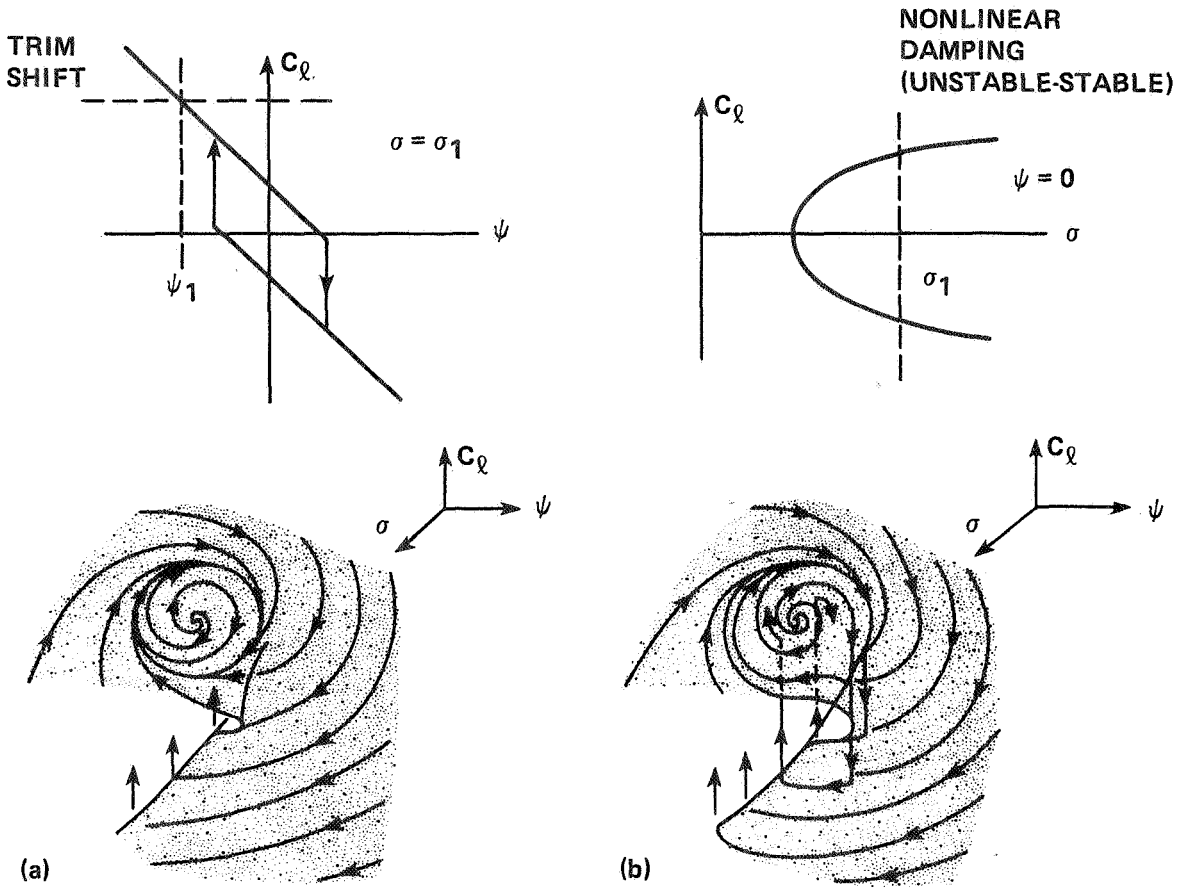
TRIM
SHIFT
C_ℓ
$\sigma = \sigma_1$
ψ
ψ_1
NONLINEAR
DAMPING
(UNSTABLE-STABLE)
C_ℓ
$\psi = 0$
σ
σ_1
C_ℓ
σ
ψ
(a)
C_ℓ
σ
ψ
(b)

Fig. 24

1. Report No.	2. Government Accession No.	3. Recipient's Catalog No.
NASA TM-85940		

4. Title and Subtitle	5. Report Date
NONLINEAR PROBLEMS IN FLIGHT DYNAMICS	May 1984
	6. Performing Organization Code

7. Author(s)	8. Performing Organization Report No.
Gary T. Chapman and Murray Tobak	A-9707
	10. Work Unit No.
9. Performing Organization Name and Address	T-6468
Ames Research Center Moffett Field, CA 94035	11. Contract or Grant No.
	13. Type of Report and Period Covered
12. Sponsoring Agency Name and Address	Technical Memorandum
National Aeronautics and Space Administration Washington, DC 20546	14. Sponsoring Agency Code 505-31-01-01-00-21

15. Supplementary Notes Originally presented as a lecture to the Berkeley-Ames Conference on Nonlinear Problems in Control and Fluid Dynamics, Univ. of California, Berkeley, Calif., May 31-June 10, 1983. Point of Contact: Gary Chapman, Ames Research Center, MS 229-3, Moffett Field, CA 94035 (415) 965-5654 or FTS 448-5654

16. Abstract

A comprehensive framework is proposed for the description and analysis of nonlinear problems in flight dynamics. Emphasis is placed on the aerodynamic component as the major source of nonlinearities in the flight-dynamic system. Four aerodynamic flows are examined to illustrate the richness and regularity of the flow structures and the nature of the resulting nonlinear aerodynamic forces and moments. A framework to facilitate the study of the aerodynamic system is proposed having parallel observational and mathematical components. The observational component consists of the elements structure, change, chaos, and scale. In the mathematical component, structure is described in the language of topology. Changes in flow structure are described via bifurcation theory. Chaos or turbulence is related to the analogous chaotic behavior of nonlinear dynamical systems characterized by the existence of strange attractors having fractal dimensionality. Scales of the flow are considered in the light of ideas from group theory.

Several one- and two-degree-of-freedom dynamical systems with various mathematical models of the nonlinear aerodynamic forces and moments are examined to illustrate the resulting types of dynamical behavior. The mathematical ideas that proved useful in the description of fluid flows are shown to be similarly useful in the description of flight-dynamic behavior. The results emphasize the importance of appreciating the strong interdependence existent between the level of knowledge of nonlinear aerodynamic phenomena, the means of mathematically modeling them, and the range of resulting flight-dynamic behavior.

17. Key Words (Suggested by Author(s))	18. Distribution Statement
Nonlinear aerodynamics Nonsteady aerodynamics Large angles of attack	Unlimited Subject Category - 02

19. Security Classif. (of this report)	20. Security Classif. (of this page)	21. No. of Pages	22. Price*
Unclassified	Unclassified	79	A05

*For sale by the National Technical Information Service, Springfield, Virginia 22161